Quantitative photoacoustic imaging study of tumours *in vivo*

Márcia Martinho Costa[1] and Anant Shah[1], Ian Rivens[1], Carol Box, Tuathan O'Shea[1], Efthymia Papaevangelou[2], Jeffrey Bamber[1] and Gail ter Haar[1]

[1]Joint Department of Physics, Division of Radiotherapy and Imaging, The Institute of Cancer Research, London and The Royal Marsden NHS Foundation Trust, Sutton, London, SM2 5PT, United Kingdom.

[2]School of Immunology and Microbial Sciences, Guy's Hospital, King's College London, London SE1 9RT, United Kingdom

Corresponding author:

Márcia Martinho Costa

email: Marcia.costa@icr.ac.uk

Address: The Institute of Cancer Research, CCI building, 15 Cotwold Road, SM2 5NG, Sutton, UK

Quantitative photoacoustic imaging study of tumours *in vivo*

Márcia Martinho Costa[1] and Anant Shah[1], Ian Rivens[1], Carol Box, Tuathan O'Shea[1], Efthymia Papaevangelou[2], Jeffrey Bamber[1] and Gail ter Haar[1]

[1]Joint Department of Physics, Division of Radiotherapy and Imaging, The Institute of Cancer Research, London and The Royal Marsden NHS Foundation Trust, Sutton, London, SM2 5PT, United Kingdom.

[2]School of Immunology and Microbial Sciences, Guy's Hospital, King's College London, London SE1 9RT, United Kingdom

Abstract: Photoacoustic imaging (PAI) provides information on haemoglobin levels and blood oxygenation (sO_2). To facilitate assessment of the variability in sO_2 and haemoglobin in tumours, for example in response to a therapy, the intrinsic variability of these parameters was evaluated in subcutaneous head and neck tumours in mice, using a PAI system (MSOT-inVision 256TF). Tumours of anaesthetized animals (midazolam-fentanyl-medetomidine) were imaged for 75 minutes; in varying positions; and repeatedly over 6 days. An increasing linear trend for tumoural haemoglobin and blood sO_2 was observed, when imaged over 75 minutes. There was no significant difference in variability of the parameters, when re-positioning tumours. A negative correlation was found between tumour growth rate and percentage decrease in blood sO_2, over 6 days. This paper shows the potential of PAI to monitor intrinsic variation and reproducibility in estimating blood sO_2 and haemoglobin, with an eventual aim of predicting and monitoring cancer treatment response.

Keywords: photoacoustic imaging; hypoxia; head and neck subcutaneous tumours; pimonidazole; blood sO_2; haemoglobin.

1. Introduction

The immature, tortuous and hyper-permeable vascular network often found in tumours, may not provide sufficient nutrients and oxygen for rapid and uncontrolled cell proliferation, which can result in regions of hypoxia, i.e. low oxygen concentration [1]. As a consequence of these structural abnormalities, blood flow in vessels fluctuates causing temporal fluctuations in the hypoxic state [2], which can occur on a time-scale of minutes or hours when they result from an efflux of red blood cells, or days when they are due to vascular network remodelling and angiogenesis [3].

Blood oxygenation may be quantified using partial pressure of oxygen (pO_2) or blood oxygen saturation (sO_2). Blood pO_2 can be measured in tissue using invasive electrodes to provide a local value. The region is considered hypoxic when pO_2 is below 10 mmHg. Blood sO_2 is an important haemodynamic parameter, defined as the ratio of oxygenated haemoglobin (HbO_2) to the total amount of haemoglobin (HbT, the sum of HbO_2 and deoxy-haemoglobin, Hb). The relationship in blood sO_2 and pO_2 is described by the oxygen-haemoglobin dissociation curve that assumes a sigmoid shape, and also describes the relationship between both parameters and oxygen concentration [4].

Hypoxia is associated with increased resistance to chemo- and radio-therapy (as extensively reviewed by [5]), two commonly used clinical cancer treatments. Assessing the spatial and temporal variation in hypoxia could be predictive of a cancer therapy response and may therefore play a critical role in treatment planning and adaptation [6, 7].

Techniques which use conventional non-invasive imaging have been developed to attempt to infer the spatial distribution of hypoxia. Several Positron Emission Tomography (PET) radiotracers are available [8-10] which are molecules that are reduced in the absence of oxygen and covalently bind to intracellular molecules, providing a non-invasive alternative, albeit with a relatively poor spatial resolution and high cost. Unfortunately, the use of radioactive isotopes is also ill-suited to longitudinal studies due to radiation dose accumulation. Blood oxygenation level dependent (BOLD) magnetic resonance imaging (MRI) [11] enables the measurement of relative blood oxygen saturation (sO_2) increase during carbogen challenge compared to air-breathing, within tumours. It has been shown that these measurements are in good spatial agreement with tissue pO_2 measurements [12-14] and histological markers of hypoxia [15, 16]. BOLD-MRI, however, has poor sensitivity and specificity and does not provide absolute sO_2.

Recently, the use of combined ultrasound (US) and optical imaging techniques, such as photoacoustic imaging (PAI), also known as optoacoustic imaging, has been proposed

as a method of non-invasively mapping blood oxygen saturation [17, 18]. PAI combines the merits of optical and ultrasound imaging, displaying optical absorption contrast with sub-millimetre spatial resolution at depths of several centimetres in tissue. Light is absorbed differentially depending on the relative concentrations of light-absorbing molecules present [19]. As a result, PAI can identify the unique spectral signatures of deoxy- (Hb) and oxy-haemoglobin (HbO_2) [17]. The quantification of the local levels of each chromophore further allows mapping of blood sO_2 distribution in the tissue [19, 20]. Low sO_2 regions tend to be hypoxic [21].

PAI has been used for hypoxia mapping pre-clinically, in subcutaneous [15, 18, 20, 22-25] and brain tumours [26], showing good agreement with pimonidazole staining [18, 22], an exogenous hypoxia marker [15], and imaging modalities, such as bioluminescence [20], high resolution and dynamic contrast enhanced ultrasound [20, 23] and BOLD-MRI [24, 25].

The PAI signal amplitude is dependent on the concentration of absorbers, the Grüneisen parameter (and consequently, tissue temperature) [17, 27, 28] [29] and local depth-dependant optical fluence [30, 31], which can introduce variability in the measurements. Regarding the depth-dependant optical fluence, the position of tissue of interest with respect to the imaging transducer can affect the measurements, as this can alter the amount of near-infrared light attenuated by overlying tissue as well as the field intensity incident on that position.

The precision of a system from the same model to that used for this paper, MSOT inVision 256-TF (iThera Medical, Germany), has been investigated in polyurethane phantoms [32]. Joseph et al. found that the mean pixel intensity of the photoacoustic image did not drift, across wavelengths of 700-1100 nm, and the coefficient of variation (CoV) of the intensity measurements over 6 hours was only 0.5% without removing the phantom between imaging acquisitions and 1.2% when the phantom was removed and replaced for imaging. When measuring the variability in mice, in healthy tissue (spleen and left kidney), the CoV for the sO_2 was less than 4% and for total haemoglobin below 18.5%, over 90 minutes continuous imaging acquisition. The group attributed this drift to the anaesthesia (isoflurane) effect in mice physiology. Joseph et al. also showed that removing and replacing the animal (6 times in one day) did not significantly affect the photoacoustic imaging measurements, resulting in CoV below 4% for the sO_2 parameter. Joseph et al. showed that *in vivo* photoacoustic imaging measurements have higher variability compared to phantoms, mostly due to the alterations in the animal's physiology resultant from the anaesthesia effect over time.

This paper aims to characterise the variability of photoacoustic imaging in subcutaneous head and neck tumours, using a commercial tomographic photoacoustic system. The

goal was to investigate the intrinsic variability in estimating the haemoglobin (Hb, HbO_2 and HbT) content of a tumour and its spatial distribution of blood oxygen (sO_2). We hypothesize tumours have a different variability from healthy tissue, due to their hypoxic nature and their growth over time. The long term application for this study would be to compare the measurements obtained here, in tumour-bearing control animals, with future studies where two cancer therapies will be used, radiotherapy and high intensity focused ultrasound (HIFU). It has been reported in the literature that both these therapies can alter the vasculature and/or the oxygenation status of tumours after being delivered, within a few days after treatment [33-35]. Therefore, this study, aims to obtain baseline measurements of the variation in the photoacoustic imaging measurements over the short term (75 minutes), to investigate the potential effects of both anaesthetic duration and altering the position of the animal, as well as over the longer term (6 days), to evaluate the variations in growing tumours.

2. Methods

2.1. Animal experiments

All research was conducted under the Guidelines of Animal Welfare provided by the UK Home Office with approval from the local animal welfare and ethics board and under Helsinki Declaration of 1975.

The human head and neck squamous cell tumour model, CAL^R, used for this study is a non-commercially available cancer cell line developed at the Institute of Cancer Research [36]. Half a million cells were injected subcutaneously into the right flank of 6 week old female $FOXnu^{n1}$ mice (~25 g). Animals were monitored for the development of a mass. Once palpable, tumour dimensions were measured every 2 or 3 days, in 3 orthogonal directions (length (l), width (w) and height (h)), using Vernier calipers. Tumour volume (V) was calculated assuming an ellipsoidal shape, commonly used for subcutaneous tumours, according to Eq. A 1.

$$V = \frac{\pi}{6} \times l \times w \times h$$

Eq. A 1

The volume error (V_{error}), for each individual tumour, was estimated from the derivative of an ellipsoidal volume, assuming a measurement error (E_m) of 0.5 mm in each direction, using Eq. A 2.

$$V_{error} = \sqrt{\left(\frac{dV}{dl} x E_m\right)^2 + \left(\frac{dV}{dw} x E_m\right)^2 + \left(\frac{dV}{dh} x E_m\right)^2}$$

Eq. A 2

Tumour dimensions are therefore presented as mean volume plus standard deviation of the estimate based only on the accuracy of the three orthogonal dimension measurements, ignoring any deviation in shape from an ellipsoid.

2.2. Tumour growth rates

Tumour growth curves were fitted to the Exponential-Linear Model to calculate tumours' growth rates [37]. The model assumes that cells initially proliferate with constant cell cycle duration, T_c, resulting in exponential growth, followed by a linear growth phase, when there is a decrease in actively proliferating cells and these are constrained to the margins of the tumour [38]. The model is described as follows:

$$\frac{\partial V}{\partial t} = \alpha_0 V, t \leq \tau$$
$$\frac{\partial V}{\partial t} = \alpha_1, t > \tau$$

Eq. A 3

where V is tumour volume (mm^3), t is time (days), α_0 is the fraction of proliferating cells at time $\ln 2/T_c$, α_1 is the growth rate in the linear phase and τ represents the time point at which the growth changes from the exponential to the linear phase. Assuming the solution is continuously differentiable then:

$$\tau = \frac{1}{\alpha_0}\log(\frac{\alpha_1}{\alpha_0 V_0})$$

Eq. A 4

where V_0 is the initial volume, in this case 0.1 mm^3, chosen as an arbitrary small initial volume of tumour cells.

The tumour growth fitting was carried out in MATLAB (2013a, 8.1.0.604), using a nonlinear least squared fit to obtain the α_0 and α_1 parameters. Fits were performed on volume data weighted using the uncertainties of each data point, which corresponded to the V_{error} calculated from Equation 2, within 95% confidence interval bounds.

2.3. Photoacoustic imaging data acquisition and reconstruction

Mice were imaged using a commercially available, real time, multispectral optoacoustic tomographic (MSOT) device, inVision 256-TF small animal scanner (iThera Medical GmbH, Munich, Germany) [30]. The system has a tunable optical parametric oscillator pumped by a Q-switched Nd:YAG near-infrared laser. A 256 element, toroidally focused, ultrasound imaging transducer (4 cm radius) with a centre frequency of 5 MHz (60% bandwidth) was used to acquire the acoustic signal, resulting from the optical tissue excitation. These

elements cover an angle of 270 degrees around the tumour to create a cross-sectional image.

Tumours were first imaged (defined as Day1) when they reached a volume of approximately 200 mm^3. Anaesthesia was induced using an intraperitoneal injection of midazolam:fentanyl:medetomidine (5.0:0.05:0.5 $mg.Kg^{-1}$). Mice were placed horizontally in a holder encased in a thin (17 μm) polyvinyl chloride (PVC) film (Fig. A 1), with their tumour facing vertically downwards, i.e. directly in the direction of the laser beam, and acoustically coupled to the membrane using ultrasound imaging gel. In order to provide acoustic coupling to the MSOT, the animal holder was completely submerged in a tank filled with 34°C distilled water. Medical air (21% oxygen) or 100%-oxygen were supplied continuously to the mouse via tubing during immersion in order to avoid asphyxiation. Imaging started approximately 5 minutes after placing the holder in the water tank, in order to allow the animal's body temperature to equilibrate with the water's temperature.

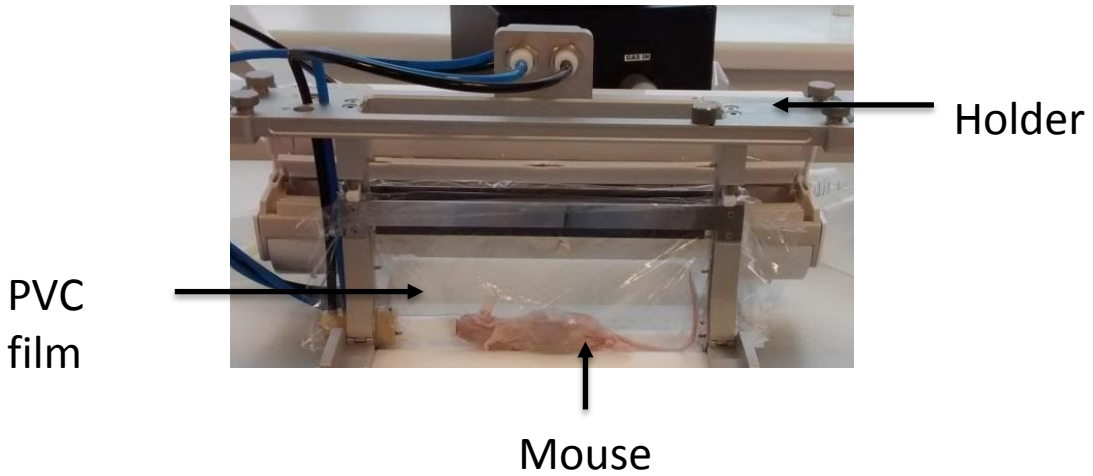

Fig. A 1: Photograph showing the experimental setup of the mouse, in the MSOT holder prior to mounting in the imaging system.

For acquiring the photoacoustic data, a volume of interest (VOI), containing the whole tumour was selected to avoid a large dataset. Transverse (medial-lateral direction) imaging slices were acquired at 1 mm intervals in the cranial-caudal direction. The optical imaging wavelengths used were: 700, 715, 730, 750, 760, 800, 850, and 900 nm. This wavelength range maximises the differences in Hb and HbO_2 signals. Ten signal averages per wavelength were obtained for each imaging slice.

Photoacoustic images were reconstructed using a model-based inversion algorithm [39] which was implemented in the viewMSOT software (v3.8) provided by iThera Medical. Spectral unmixing was used to calculate the contribution of each chromophore, oxy- and deoxy-haemoglobin, in blood, in order to calculate the oxygen saturation. This is done on a

pixel-by-pixel basis, through a linear regression algorithm [40]. The software subsequently allows calculation of the mean oxy- (HbO_2) and deoxy-haemoglobin (Hb) signals in a user defined region of interest (ROI) which could be drawn onto the greyscale anatomical image (Fig. A 2A). These mean Hb and HbO_2 values are added together to calculate the mean total haemoglobin per ROI. For any ROI the mean oxygen saturation was calculated using Eq. A 5.

$$mean\ sO_2 = \frac{mean\ (HbO_2)}{mean\ (Hb) + mean\ (HbO_2)}$$

Eq. A 5

All the parameters are unitless quantities, described in arbitrary units (A.U.), because the software does not take use light fluence and the system response in calculations, which would be necessary to quantify the concentration (in mmol/L or mg/L) of each chromophore.
The viewMSOT software also allows mapping of the spatial distribution of sO_2 calculated on a pixel-by-pixel basis, an 'oxymap' (Fig. A 2B). Black pixels in such images indicate where the total amount of haemoglobin is below the noise threshold. The intensity of such pixels is set to zero. The software automatically provides the percentage of black pixels per ROI.

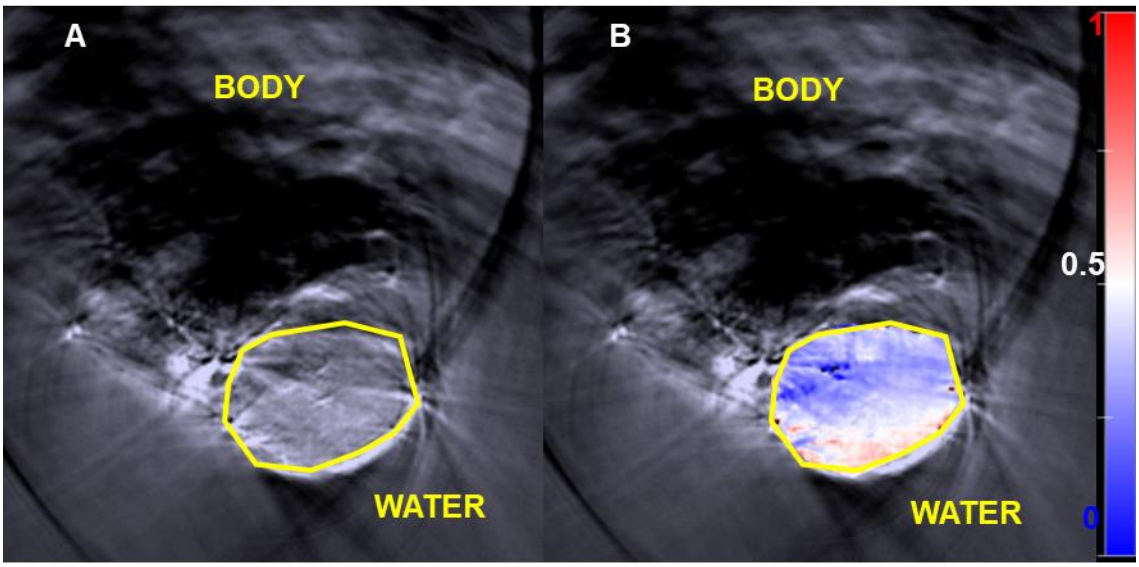

Fig. A 2: A: Greyscale anatomical photoacoustic image obtained from optical excitation at a single wavelength (800 nm). The yellow polygon is the ROI used to delineate the tumour. B: Shows an 'oxymap' overlaid on the tumour. The 'oxymap' colour scale on the right represents the blood sO_2 calculated by the MSOT software on a pixel-by-pixel basis. Blue represents sO_2 <0.5 A.U (white), while red is sO_2 >0.5 A.U. Black pixels within the ROI show where haemoglobin signals are below the noise threshold.

2.4. Imaging studies

Three separate imaging studies were performed.

The first was a short term MSOT study designed to investigate any potential effects of anaesthesia on total haemoglobin and blood sO_2. A 3D whole tumour dataset was acquired every 5 minutes for 75 minutes after allowing 5 minutes for the tumour to reach thermal equilibrium with the imaging system. Only air-breathing imaging was acquired, in order to maximise the rate (and number) of datasets that could be acquired. Measurements were acquired in 4 animals when their tumours reached a target volume of 200 mm^3.

In order to study how re-positioning the animal affects measurements of blood haemoglobin and blood sO_2, a second short term study was performed, 24 hours later. The same 4 animals were anaesthetised once and imaged in three consecutive sessions after being dismounted from the imaging system between each session. In addition, their tumour was placed at a slightly different position relative to the transducer each time. Whole tumour 3D datasets were acquired first under air- breathing conditions which took approximately 2 minutes, and then under 100% oxygen-breathing, after allowing 2 minutes for the oxygen to reach the tumour, for the same VOI, under hyperoxic conditions [25]. Oxygen can be used as a contrast agent for PAI, by highlighting spatial differences in vascularity [41]. Approximately 4 minutes were needed to remove the animal from the holder, reposition it and replace it (see Fig. A 3).

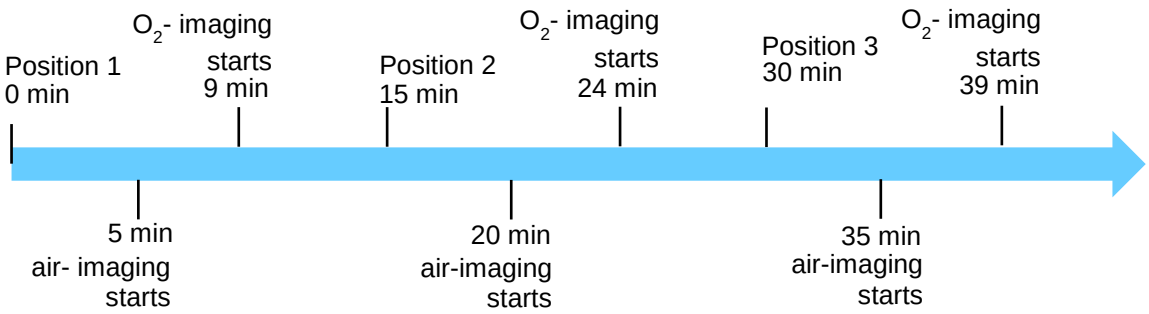

Fig. A 3: Diagram for the re-positioning of the animal (bottom arrow). Each imaging session started at approximately 5, 20 and 35 minutes after placing the animal in the water tank of the MSOT system, during air-breathing. Air-breathing imaging takes approximately 2 minutes. The air is then changed for 100 %-O_2, for 2 minutes and the same region is re-imaged for approximately 2 minutes again, during O_2-breathing.

For both short-term studies, a linear regression model was applied to calculate an estimate of the average change in signal over time, as well as the goodness of fit between the imaging data and the model. This was obtained using the curve fitting toolbox (version 3.5.3) available in MATLAB R2016a software. To investigate the suitability of the linear model for these studies, three parameters were calculated: goodness of fit (R^2) that indicates how much of the variability of the parameter (Hb, HbO_2, HbT and sO_2) is time-dependent; p-value of the model represents if the slope is significantly different from 0 (if p-value<0.05); and the Sum of Squared Errors (SSE) of the prediction model that indicates the suitability of the

linear model to explain the variability behaviour of the data (the closer SSE is to 0, the better the linear fitting).

The third, a long-term study was designed to sequentially image tumours during a period of growth. When tumours (n=10) reached a volume of approximately 200 mm^3, animals were imaged on 3 consecutive days ('day 1, 2 or 3'). This volume was chosen as being suitable for future studies of cancer treatment e.g. using radiotherapy. Tumours were also imaged on day 6 in order to evaluate changes in haemoglobin and blood sO_2 during tumour growth. For this study, animals were imaged under air- and oxygen-breathing conditions.

For short- and long-term studies, three slices in each tumour, separated by 1 mm, were chosen for analysis, a central slice and the adjacent slice on either side. The mean haemoglobin and blood sO_2 values were obtained by averaging over the three whole-tumour ROIs to provide the tumour ROI-averaged Hb, HbO_2, HbT and sO_2. For each animal, the average percentage of black pixels in the three central tumour slices was also calculated in order to evaluate the signal lost in each ROI.

2.5. Immunohistochemistry

Five tumours were collected after imaging for immunohistochemistry, including pimonidazole staining that binds to hypoxic ducts, and H&E to analyse tissue structure. Pimonidazole was administered to the animal intraperitoneally (60 mg/kg) 45 minutes before sacrificing it. Tumour samples were excised and immediately snap frozen on dry ice and stored at -80°C until sectioning.

For H&E staining, frozen tumour sections (10 µm thick) were counterstained in 'Harris' haematoxylin (dyes cellular nuclei) and eosin (dyes cytoplasm and organelles). Samples were then dehydrated with a sequence of ethanols and xylene, and mounted using DPX mounting medium (Sigma-Aldrich, Dorset, UK). Acetone-fixed cryosections (consecutive to the ones used for H&E) were used to visualize pimonidazole adduct formation with an anti-pimonidazole FITC-conjugated mouse monoclonal antibody (1:200) (Hypoxyprobe™ Plus kit, Hypoxyprobe, Inc., Burlington, USA).

Stained sections were imaged using a BX51 microscope (Olympus Optical, London, UK), with a motorised stage (Prior Scientific Instruments, Cambridge, UK), driven by microimaging software (cellSens, Olympus Optical, London, UK). This allows automatic acquisition of the full sample. Microscopic images were acquired using a digital camera (ColorView 12; Soft Imaging System GmbH, Munster, Germany) and exposure times of 100 ms (H & E) or 500 ms (pimonidazole) using a x4 objective.

2.6. Statistical analysis

The slice-, intra-tumour and inter-tumour coefficients of variation (CoVs), i.e. the ratio of standard deviation to mean, were calculated for Hb, HbO_2, HbT and sO_2 in all PAI studies. The first indicates how much variation to expect between the 3 ROIs chosen for the analysis of the PAI parameters; the second the variation of the measurements for each animal and the third the variation between animals.

A paired student t-test was used to assess the level/degree of significance of differences in the mean Hb, HbO_2, HbT and sO_2 of CAL^R tumours during the long term variability studies, on imaging days 1, 2, 3 and 6, using R software.

3. Results

3.1. Comparison between photoacoustic imaging and immunohistochemistry

Pimonidazole staining indicates the presence of widespread perfusion-limited or diffusion-limited hypoxia (Fig. A 4 B and E) with unstained regions largely corresponding to necrotic/acellular regions, observed in the H&E staining (Fig. A 4 A & D) and avascular (black or very dark blue) regions on the PAI 'oxymaps'. The blue pixels in tumour 'oxymaps' (Fig. A 4 C and F) corresponding to low sO_2 (<0.5), spatially correlated to tumour hypoxia, as determined using pimonidazole staining. Red pixels in the tumour 'oxymaps', e.g. the periphery of the tumour in Fig. A 4 C, generally corresponded with weak/negative pimonidazole staining (Fig. A 4 B). Albeit, a small proportion of the red oxymap pixels (particularly in Fig. A 4 C), correspond with pimonidazole staining, indicating hypoxia.

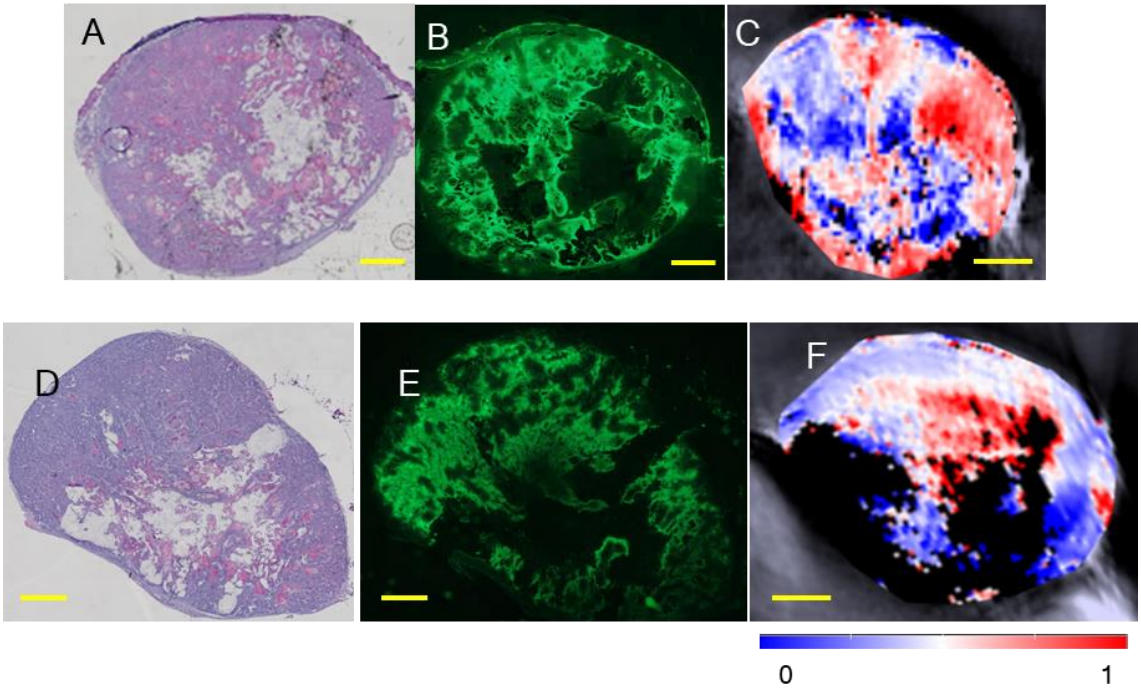

Fig. A 4: Representative examples of 2 CAL^R tumours (volumes of 220±12 mm^3, top, and 221±28 mm^3, bottom). A&D: H&E staining, B&E: pimonidazole staining and C&F: 'oxymaps' of corresponding central tumour slices.

3.2. Short term PAI variability study

3.2.1. Variation in time over 75 minutes

For the first short-term study, aimed to investigate the anaesthesia effect over 75 minutes in the photoacoustic imaging measurements, four animals were imaged. Fig. A 5 shows the short term variation in the ROI-averaged percentage of black pixels and average Hb, HbO_2, HbT and sO_2, over the three tumour slices per animal. A trend for a decrease in the percentage of black pixels (i.e. those with undetectable levels of haemoglobin), is observed for animals 1, 2 and 4 after the initial 10 minutes of imaging, after an initial increase between 5 and 10 minutes. Animal 3 has a more constant percentage of black pixels compared to the remaining 3 animals, over the 75 minutes of imaging. An increase in Hb and HbO_2 (and therefore HbT), and sO_2 over the whole time period was observed for all tumours, except for the sO_2 values measured for animal 3. The different change rates are quantified in Table A 1.

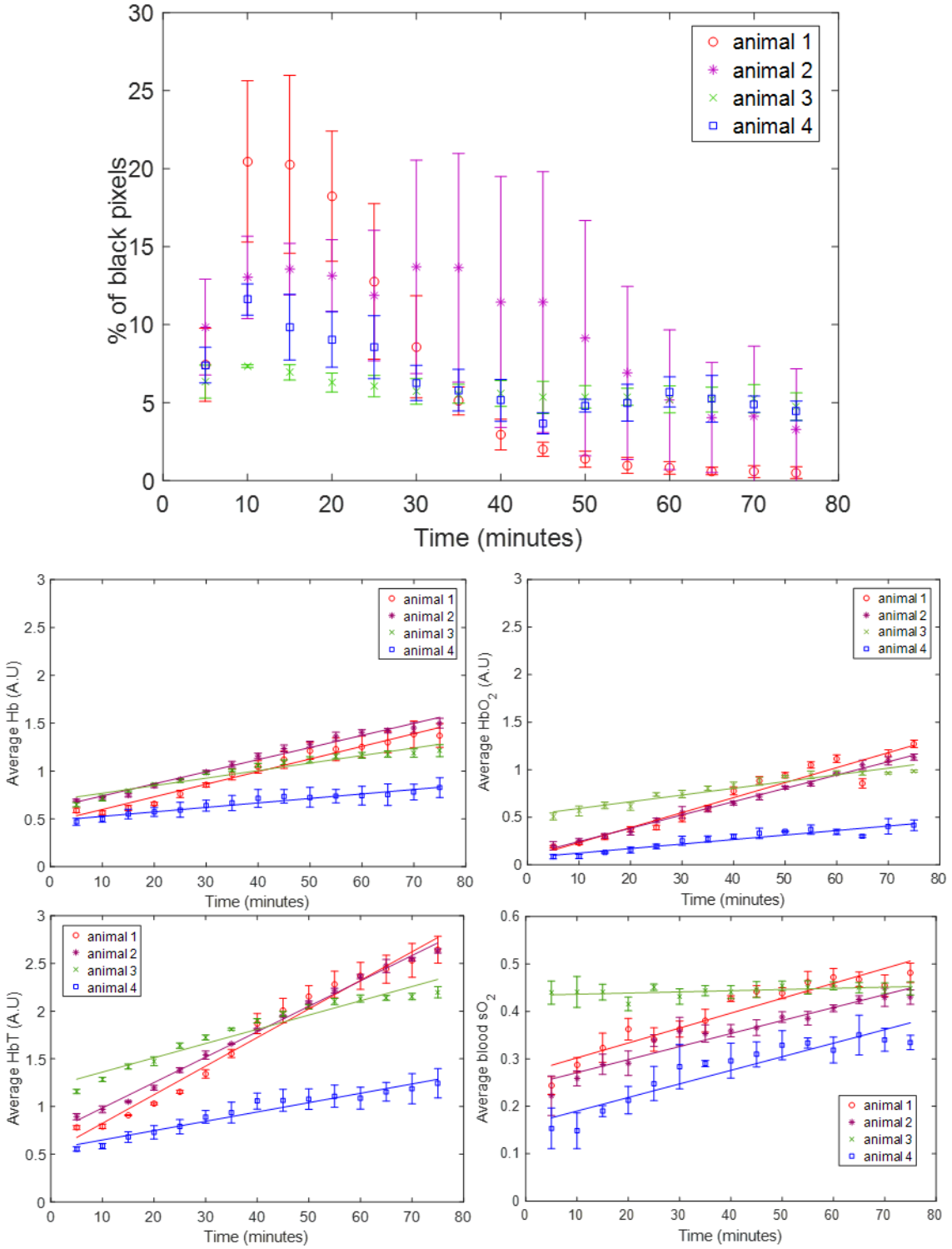

Fig. A 5: ROI-averaged percentage of black pixel, and Hb, HbO_2, HbT and sO_2 signals, for CAL^R tumours (n=4) imaged over 75 minutes, during air-breathing. Error bars represent the standard deviation over 3 adjacent central tumour slices, 1 mm apart. Solid lines represent a linear regression fitted to the data.

Table A 1 summarises the ROI-averaged rate of change of Hb, HbO_2, HbT and sO_2, as well as the goodness of fit (R^2) and the sum of squares of error (SSE) of the linear regression

used to calculate these rates of signal change. Animals 1 and 2 had a faster increase in Hb and HbO_2 than animals 3 and 4. This was reflected in the rate of HbT over 75 minutes. While for animals 1 and 2, the increase in HbT was above 0.027 min^{-1}, for animals 3 and 4, the increase rate for this parameter was <0.015 min^{-1}.The table also shows the increase in blood sO_2. Animals 1, 2 and 4, had similar increases in blood sO_2 (range: 0.0027-0.0031), but for animal 3, the blood sO_2 rate of change was negligible, 0.00025 (3.148e-05, 0.00047), as indicated by a low R^2 value, 0.267, representative of a more horizontal line. This is a consequence of a similar increase in Hb (0.0079 min^{-1}) and HbO_2 (0.0071 min^{-1}). Table A 1 also shows that the SSE parameter for the linear model applied was generally below 0.05, indicative of a good agreement between the calculated model and the measured data. Exceptions are the resultant SSE for the linear model used in ROI-averaged HbO_2 and HbT data of animal 1 and ROI-averaged HbT data of animal 2.

Table A 1: Rate of change of ROI-averaged Hb, HbO_2, HbT and sO_2 signal during the short-term (75 minutes) longitudinal study. The goodness of fit, R^2, indicates how much of the signal variability is time dependent and the p-value if the signal change (slope of the linear model) is significantly different from zero. The SSE reflects how similar the predicted values and measured data are, i.e. the closest SSE is to zero, the better the linear fit.

Animal		Signal change, min^{-1} (95% CI)	R^2	p-value	SSE
1	Hb	0.013 (0.012, 0.015)	0.971	<0.0001	0.037
	HbO_2	0.016 (0.013, 0.018)	0.932	<0.0001	0.117
	HbT	0.030 (0.027, 0.033)	0.976	<0.0001	0.142
	sO_2	0.0031 (0.0025, 0.0038)	0.895	<0.0001	0.007
2	Hb	0.013 (0.013, 0.014)	0.981	<0.0001	0.020
	HbO_2	0.014 (0.013, 0.015)	0.995	<0.0001	0.006
	HbT	0.027 (0.026, 0.028)	0.995	<0.0001	0.027
	sO_2	0.0027 (0.0023, 0.0032)	0.923	<0.0001	0.004
3	Hb	0.0079 (0.0066, 0.0091)	0.930	<0.0001	0.030
	HbO_2	0.0071 (0.0060, 0.0082)	0.934	<0.0001	0.023
	HbT	0.015 (0.013, 0.017)	0.938	<0.0001	0.096
	sO_2	0.00025 (3.148e-05, 0.00047)	0.267	0.027	0.001
4	Hb	0.0047 (0.0040, 0.0054)	0.940	<0.0001	0.009
	HbO_2	0.0047 (0.0038, 0.0057)	0.895	<0.0001	0.017
	HbT	0.0098 (0.0084, 0.011)	0.940	<0.0001	0.039
	sO_2	0.0029 (0.0022, 0.0035)	0.857	<0.0001	0.009

The average slice-CoV, intra- and inter-tumour CoVs in ROI-averaged Hb, HbO_2, HbT and sO_2, over the 75 minute acquisition for each animal, are summarised in Table A 2. Overall, the intra-tumour CoV was higher for the haemoglobin components (>22.5±6.0%) than for sO_2 (16.0±8.4%). The slice-CoV, indicative of the variation of photoacoustic imaging parameters, in the 3 ROIs chosen for each tumour, was lowest for all the parameters (<13.9±7.4%) compared to the intra-tumour CoV.

Table A 2: Summary of slice- and intra-tumour CoV of the measurements of each animal acquired over 75 minutes, and the average Hb, HbO_2, HbT and sO_2 measured during that time period.

Animal	ROI-averaged Parameter	average±std	Intra-tumour CoV (%)	Average slice-CoV (%)
1	Hb	0.99±0.30	30.1	6.4±2.6
	HbO_2	0.71±0.36	51.5	5.5±1.9
	HbT	1.72±0.68	39.3	4.2±2.2
	sO_2	0.40±0.07	18.7	5.0±2.1
2	Hb	1.12±0.29	25.5	2.4±0.8
	HbO_2	0.66±0.31	47.1	6.5±5.4
	HbT	1.78±0.60	33.5	1.5±1.2
	sO_2	0.35±0.06	18.0	5.6±4.2
3	Hb	1.00±0.18	18.1	2.5±1.2
	HbO_2	0.80±0.16	20.3	4.0±2.4
	HbT	1.81±0.34	19.0	1.7±0.6
	sO_2	0.44±0.01	2.2	3.3±1.5
4	Hb	0.67±0.11	16.2	10.9±2.6
	HbO_2	0.27±0.11	41.9	13.9±7.4
	HbT	0.94±0.23	23.9	9.3±2.5
	sO_2	0.28±0.07	24.9	11.5±7.4
Average intra-CoV (n=4)	Hb	22.5±6.5		
	HbO_2	40.2±13.9		
	HbT	22.9±9.2		
	sO_2	16.0±8.4		

The inter-tumour CoV calculated for this study was 20.9±3.1% for Hb, 46.4±12.4% for HbO_2, 28.6±2.3% for HbT and 21.8±10.9% for sO_2. The largest variation was measured for HbO_2. These results show that, for the short-term longitudinal study, inter- and intra-tumour CoV

were similar, showing a high variability expected for each animal when imaged over 75 minutes.

3.2.2. Re-positioning study

The results for the study on the effect of repositioning 4 animals three times in the photoacoustic system are shown below. The trends for air- and oxygen-breathing were similar, so the results for air-breathing are shown here and the results for oxygen-breathing are in the supplemental data section (Fig. B1 and Tables B1 and B2).

The oxymap of the central tumour slice for each mounting position for each CAL^R tumour is shown overlain on greyscale anatomical images in Fig. A 6. The tumour of animal 1 had mostly low blood sO_2, <0.5, as indicated by the blue regions (see colour scale), for positions 1 and 3, with the 'oxymap' for position 2 indicating some regions with medium to high blood sO_2 (>0.5), represented in white, pink and red. For animals 2 and 3, the centre of the tumour had mostly low blood sO_2 (in blue). In the margins of the tumours, white to red pixels are observed, indicative of medium to high blood sO_2. For animal 3, tumour positions 2 and 3 were similar, as well as the respective 'oxymaps'. On the bottom row, it is possible to see that the blood sO_2 of animal 4 is low, and in position 2, the 'oxymap' of the central slice of the tumour shows a large region of black pixels (41%). In positions 1 and 3, some white to red pixels are observed, again close to the margins of the tumour.

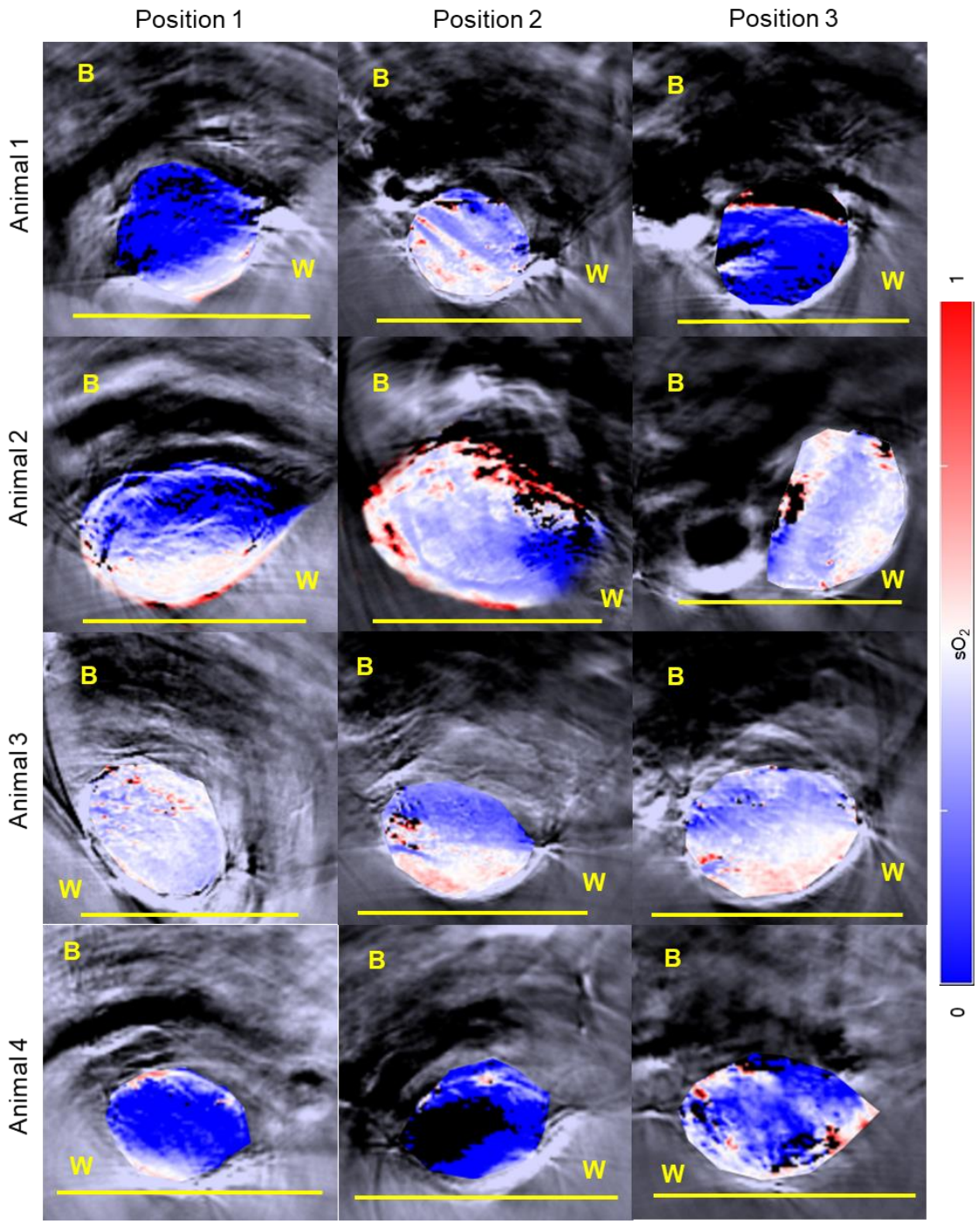

Fig. A 6: sO_2 distributions or 'oxymaps' of 4 CAL^R tumours, positioned differently by remounting the animals 3 times in the MSOT tank with the minimum time interval between each imaging session (see Fig. A 2). The 'oxymaps' are shown as overlays on greyscale photoacoustic images, of the central slice of each tumour. B: body; W: water Yellow bar represents a 10 mm size scale.

Following the changes observed in the 'oxymaps' in Fig. A 6, the changes in the ROI-averaged Hb, HbO_2, HbT, sO_2 and percentage of black pixels, were analysed over imaging time, in order to investigate if re-positioning of animal had an additive effect to the time the animal is under anaesthesia in the variability of the parameters analysed.

Fig. A 7 shows the ROI-averaged percentage of black pixels for each animal, in each of the three imaging positions, for the 3 central slices. While for the majority of the tumours the mean percentage of black pixels (undetectable haemoglobin levels) was below 19%, animal 4, in position 2, had an abnormally high proportion of black pixels, 46±8%. Fig. A 7 also shows that re-positioning the animals resulted in statistically different measurements of haemoglobin content and calculated blood sO_2 levels. A trend for an increase in ROI-averaged Hb, HbO_2 and HbT was observed for all animals over time, independently of the starting and ending angle of the tumour relative to the transducer, apart from animal 4 in position 2, where a high percentage of black pixels was measured. A trend for increasing in ROI-averaged blood sO_2 levels was also observed for animals 3 and 4, remaining more constant for animals 1 and 2.

The quantification of the changes in signal, both for the individual haemoglobin components and blood sO_2, is shown in Table A 3. For animal 3, since the blood sO_2 remained constant, R^2 was low (0.189), although SSE was also very low (<0.001), showing a good linear fit. The R^2 for the linear regression model applied in the re-positioning study for animal 4 was low for the blood sO_2 (0.153) and for individual haemoglobin components, <0.289. From Fig. A 7, it is possible to that, for this animal, position 2 had abnormally low haemoglobin and sO_2 values, which can explain the poor goodness of fit. The p-values in Table A 3 show that the slopes, i.e. changes in signal over time, for Hb, HbO_2, HbT and SO_2, were not significantly different from zero.

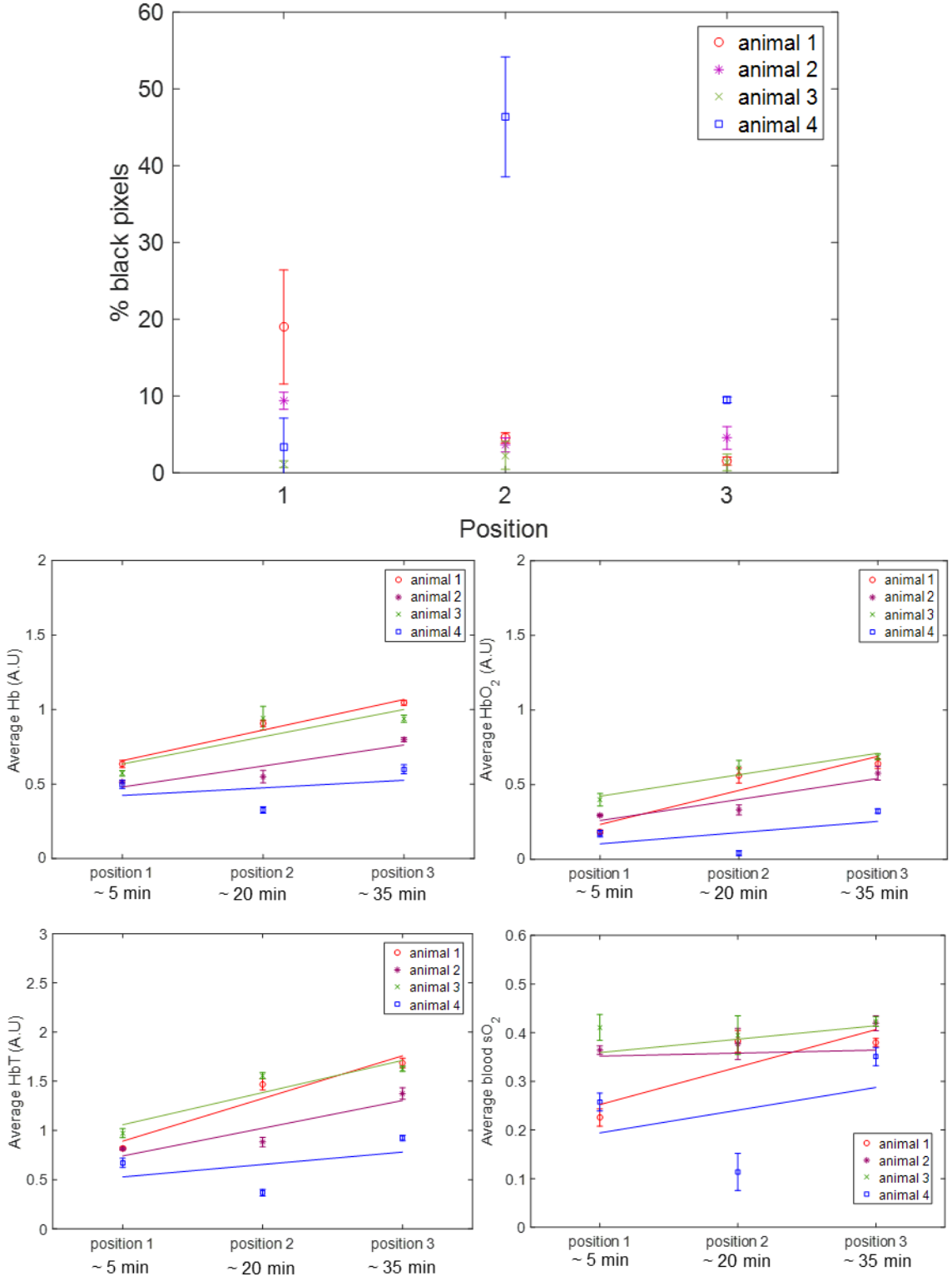

Fig. A 7: ROI-averaged percentage of black pixel, and Hb, HbO_2, HbT and sO_2 signals, for CAL^R tumours (n=4) imaged after being removed and re-positioned in the tank three times, during air-breathing. Error bars represent the standard deviation over 3 adjacent central tumour slices, 1 mm apart. Solid lines represent a linear regression fitted to the data.

Table A 3: Rate of change of ROI-averaged Hb, HbO_2, HbT and sO_2 signal during the re-positioning study (air-breathing). The goodness of fit, R^2, indicates how much of the signal variability is time dependent and the p-value if the signal change (slope of the linear model) is significantly different from zero. The SSE reflects how similar the predicted values and measured data are, i.e. the closest SSE is to zero, the better the linear fit.

Animal	Signal change, min^{-1} (95% CI)		R^2	p-value	SSE
1	Hb	0.014 (-0.019, 0.047)	0.966	0.120	0.003
	HbO_2	0.015 (-0.058, 0.089)	0.874	0.230	0.015
	HbT	0.030 (-0.077, 0.14)	0923	0.179	0.031
	sO_2	0.0051 (-0.034, 0.044)	0.738	0.340	0.004
2	Hb	0.0094 (-0.043, 0.062)	0.837	0.265	0.008
	HbO_2	0.0094 (-0.042, 0.060)	0.846	0.256	0.007
	HbT	0.019 (-0.085, 0.12)	0.841	0.262	0.030
	sO_2	0.0018 (-0.0055, 0.0092)	0.911	0.188	<0.001
3	Hb	0.012 (-0.079, 0.10)	0.742	0.339	0.023
	HbO_2	0.0096 (-0.025, 0.044)	0.927	0.174	0.003
	HbT	0.022 (-0.10, 0.15)	0.829	0.271	0.043
	sO_2	0.00041 (-0.010, 0.011)	0.189	0.018	<0.001
4	Hb	0.0034 (-0.11, 0.11)	0.136	0.762	0.033
	HbO_2	0.0050 (-0.096, 0.11)	0.289	0.639	0.028
	HbT	0.0084 (-0.20, 0.22)	0.207	0.700	0.122
	sO_2	0.0031 (-0.090, 0.096)	0.153	0.155	0.024

No statistical differences were found between the signal change calculated for the repositioning study and that obtained for the longitudinal (75 minute) study, for ROI-averaged Hb, HbO_2, HbT and sO_2, apart for the HbT parameter for animal 2. Figs. B2-B5 show the longitudinal and re-positioning data for Hb, HbO_2, HbT and SO_2, for each animal, plotted in the same figure and the p-values showing the similarity of the slopes, i.e. if p-value<0.05 the change in signal was significantly different between the 75 minute and re-positioning studies. The slice- and intra-tumour CoVs for ROI-averaged Hb, HbO_2, HbT and sO_2, are summarised in Table A 4. The intra-tumour CoV measurement of animal for, excluding position 2, where 46% of signal was lost, is also shown. As was seen for the 75 minute studies, the intra-CoV for measurements acquired after re-positioning the animals was higher for the haemoglobin components (>22.0±6.0%) than for the sO_2 (22.0±21.2 and

15.0±11.3 with and without considering position 2 imaging for animal 4, respectively). The slice-CoV was also lower (19.4±18.4% including animal 4, position 2 imaging) compared to the intra-CoV.

Table A 4: Summary of average slice- and intra-tumour CoV of the measurements after repositioning each animal 3 times, during air-breathing imaging, and the average Hb, HbO_2, HbT and sO_2.

Animal	Parameter	average (±std)	Intra-tumour CoV (%)	Average Slice-CoV (%)
1	Hb	0.86±0.21	24.3	2.6±1.2
	HbO_2	0.46±0.24	52.7	6.9±2.1
	HbT	1.32±0.45	34.0	2.9±1.0
	sO_2	0.33±0.09	27.3	5.3±2.9
2	Hb	0.62±0.15	24.8	3.7±3.4
	HbO_2	0.40±0.15	38.1	7.1±3.6
	HbT	1.02±0.31	30.0	3.7±2.1
	sO_2	0.39±0.03	7.5	4.9±3.2
3	Hb	0.82±0.21	26.0	4.7±3.2
	HbO_2	0.57±0.15	26.4	7.1±3.9
	HbT	1.38±0.36	25.9	2.8±1.7
	sO_2	0.41±0.01	3.4	6.3±3.8
4	Hb	0.47±0.14	29.1	5.6±0.8
	HbO_2	0.18±0.14	78.3	19.4±18.4
	HbT	0.65±0.28	42.5	6.5±3.1
	sO_2	0.24±0.12	49.7	15.4±15.8
4 (excluding position 2)	Hb	0.55±0.07	13.1	5.1±0.2
	HbO_2	0.25±0.11	42.9	9.0±5.8
	HbT	0.80±0.18	22.4	5.1±2.8
	sO_2	0.30±0.07	21.7	6.3±1.3
Average intra-tumour CoV (n=4)	Hb	26.0±2.2		
	HbO_2	48.9±22.4		
	HbT	33.1±7.1		
	sO_2	22.0±21.2		
Average intra-tumour CoV (without position 2 for mouse 4) (n=4)	Hb	22.0±6.0		
	HbO_2	40.0±11.0		
	HbT	28.1±5.1		
	sO_2	15.0±11.3		

Including the data point for animal 4, position 2, the inter-CoV calculated was of 25.8±16.4% for the average Hb, 45.6±19.6% for the average HbO_2, 30.6±15.6% for the average HbT and 26.5±8.3% for the average sO_2. Excluding that data point, the inter-CoV calculated was of

20.4±16.4% for the average Hb, 33.2±6.4% for the average HbO_2, 22.7±6.8% for the average HbT and 13.0±13.2% for the average sO_2.

3.3. Variation during tumour growth, 6 day study

For the long-term studies, 10 CAL^R tumours were imaged. The ROI-averaged Hb, HbO_2, HbT and sO_2 from 3 central slices per tumour, measured during air-breathing, for the long term (6 day) variability study (total of 4 imaging sessions) are shown in Fig. A 8. There was no statistically significant persistent increase or decrease in Hb, HbO_2, HbT, or sO_2 over the 6 days, with the exception of a statistically significant decrease in Hb, from 1.25±.0.4 A.U. to 0.9±.0.2 A.U., from day 1 to 3.

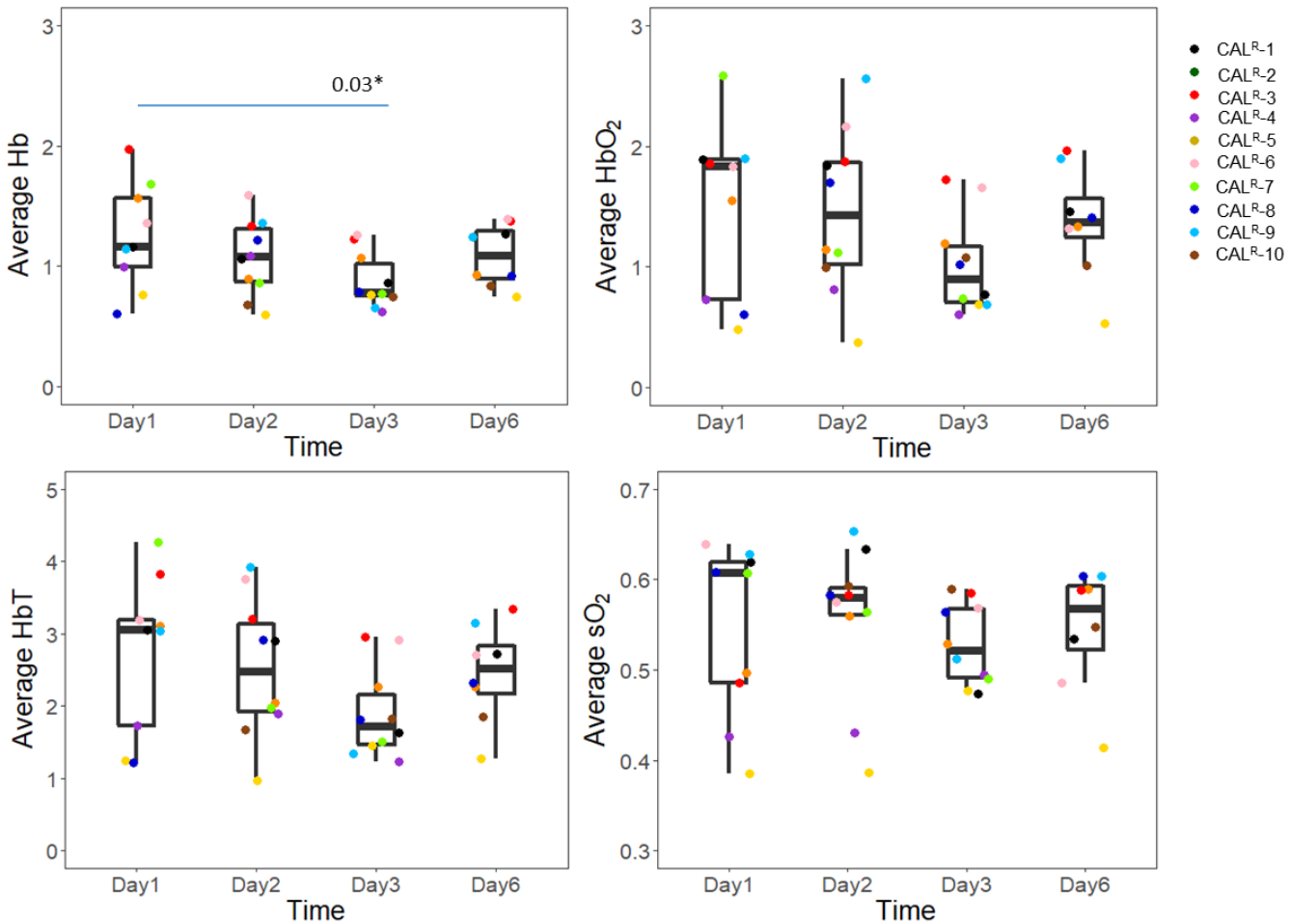

Fig. A 8: Average haemoglobin and blood sO_2 values for the 3 central tumour slices of 10 CAL^R tumours, over a 6 day imaging period, for air-breathing imaging. Day 1 corresponds to the time at which tumours reached approximately 200 mm^3. The whisker plots shows the distribution of the measurements; the central black line in each box represents the median of the population; top and bottom horizontal lines in each box represent the upper and lower quartile and the whiskers the minimum and maximum values.

The oxygen-breathing results are similar and are included in the supplemental data (Fig. B7 and Table B3).

The inter- and intra-tumour CoV for air-breathing photoacoustic imaging, for 4 imaging sessions acquired over 6 days, are summarised in Table A 5. As was found for the short term variability studies, the intra- and inter-tumour CoV for the sO_2 parameter was lower (7.5±2.5% and 13.1±3.2%, respectively) comparatively to haemoglobin parameters (range 19.3±8.7% to 39.7±5.6%).

Table A 5: Summary of inter- and intra-tumour CoVs for the CAL^R tumours (N=10), over a 6 day period, for ROI-averaged Hb, HbO_2, HbT and sO_2, during air-breathing imaging.

Parameter	Intra-tumour CoV (%)	Inter-tumour CoV (%)
Hb	19.3±8.7	27.0±4.1
HbO_2	22.8±15.4	39.7±5.6
HbT	20.6±12.0	32.7±4.7
sO_2	7.5±2.5	13.1±3.2

3.4. Tumour growth rate

Growth rates calculated for ten CAL^R tumours used in the longitudinal study are shown in Table 6. The individual fitted growth curves, as well as the exponential-linear model fitting, are shown in the Supplemental Data (Fig. B6). The uncertainties (95% confidence intervals) are large and hence no statistically significant difference was found between individual tumour growth rates. The goodness of fit, R^2, for the majority of the tumours (N=8) is ≥ 0.88, suggesting good agreement between the exponential-linear model and the data. Animals CAL^R-1 and CAL^R-8, had abnormally low fits to the model. CAL^R-1 ulcerated, which can affect the tumour growth (see Fig. B6). Fig. B6 shows stagnated tumour growth (108±18 mm^3 to 123±20 mm^3) between days 12 to 20 after tumour implantation for CAL^R-8.

Table A 6: Exponential (α_0) and linear (α_1) growth rates, and time after implantation for transition between exponential and linear phase, τ, for 10 CAL^R tumours, including the goodness of fit of the exponential-linear model to the growth curves.

Mouse	α_0 (day^{-1})	95% confidence interval for α_0	α_1 ($mm^3.day^{-1}$)	95% confidence interval for α_1	τ (days after tumour implant)	Goodness of fit (R^2)
CAL^R-1	0.55	[0.24; 0.85]	23	[0.48; 45]	5	0.77
CAL^R-2	0.53	[0.41; 0.65]	46	[29; 63]	6	0.92
CAL^R-3	0.48	[0.28; 0.68]	11	[8; 14]	5	0.90
CAL^R-4	0.48	[0.36; 0.60]	10	[9; 12]	5	0.95
CAL^R-5	0.48	[0.36; 0.60]	48	[16; 79]	6	0.88
CAL^R-6	0.66	[0.52; 0.81]	55	[38; 72]	4	0.97
CAL^R-7	0.50	[0.43; 0.56]	26	[21; 32]	5	0.99
CAL^R-8	0.33	[0.26; 0.39]	49	[0; 110]	10	0.64
CAL^R-9	1.2	[0; 2.7]	10	[7; 12]	2	0.95
CAL^R-10	0.77	[0.22; 1.3]	30	[18; 42]	3	0.96

Table A 6 shows that the time at which tumour growth changes from exponential to linear varies from 2 to 10 days after tumour implant. Based on these results and the growth curves shown in Fig. B6, all photoacoustic imaging acquired for this study was performed during linear growth. In Fig. A 8, the change in blood sO_2 over the 6 days of imaging did not follow the same trend for all tumours, i.e. there was no statistically significant persistent increase or decrease in blood sO_2 between day 1 and day 6 of imaging. In order to investigate if these changes were related with change in volume over time (ΔV), calculated using raw caliper volume measurements, or linear rate of tumour growth (α_1), estimated using the exponential-linear model, the relationship between these parameters and the percentage difference in sO_2 between day 6 and day 1 was investigated and it is shown in Fig. A 9. It is possible to observe a good negative correlation between the percentage difference in sO_2 and both ΔV and α_1, but only during oxygen-breathing, i.e. the larger the change in sO_2 (oxygen-breathing), the faster the tumour was growing.

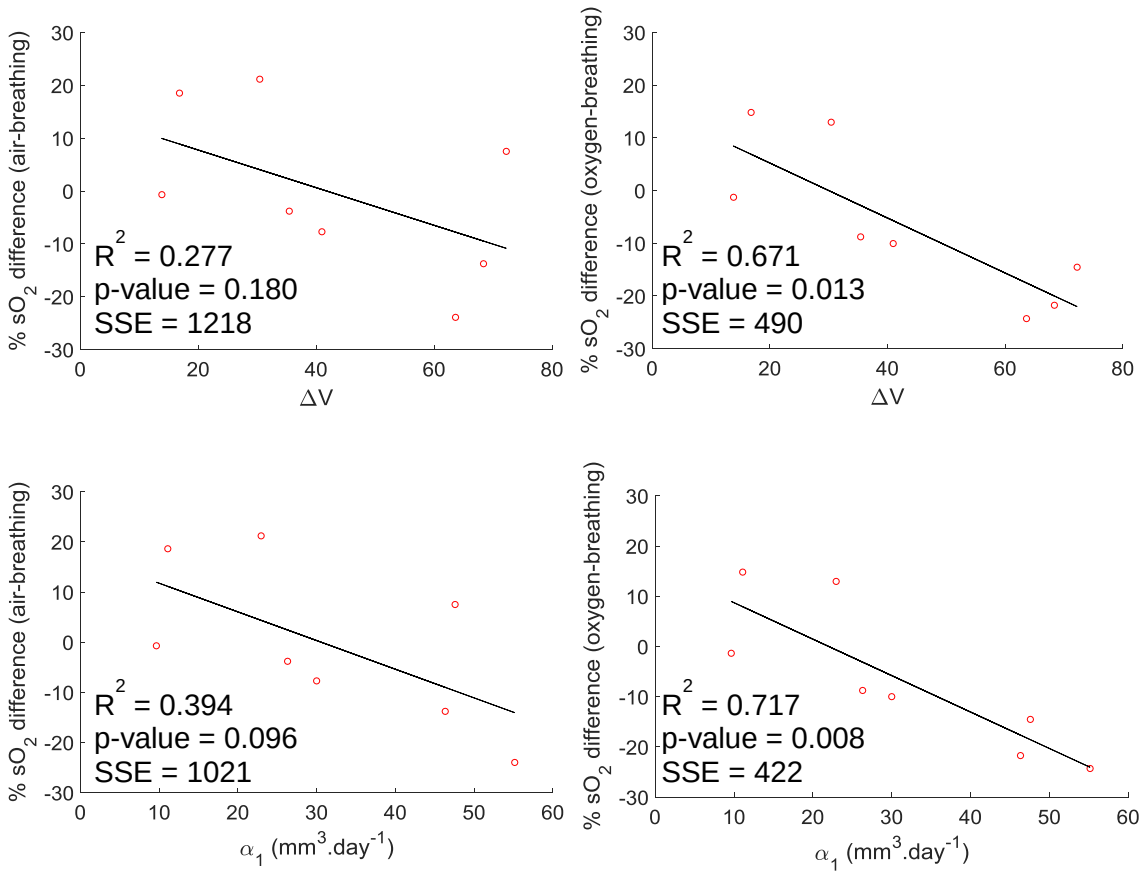

Fig. A 9: Correlation between rate of change in volume between day 1 and 6 of imaging, ΔV, or linear growth rate, $\alpha 1$, and the percentage difference in sO_2 between days 1 and 6 of imaging for 8 CAL^R tumours, for air- and oxygen-breathing measurements.

4. Discussion

The main objective of this paper was to explore the intrinsic variability of the sO_2, HbO_2, Hb and HbT parameters in subcutaneous head and neck tumours, as measured using a tomographic photoacoustic system, over short periods of time (minutes-hours), longer periods (several days), and by re-positioning the animals in the imaging cradle. From these studies, it is possible to quantitatively investigate the variability due to anaesthesia, tumour growth and re-positioning in consecutive imaging sessions, respectively. The results of this study can directly feed into follow-up studies that would involve assessing the variability of these parameters in response to radiotherapy and/or HIFU.

Initially, the spatial correspondence between photoacoustic images and histology staining for hypoxia was investigated (Fig. A 4). For this study, pimonidazole, a well-established exogenous marker of hypoxia, was used [42, 43]. Gerling et al. [18] had showed good agreement (R^2 = 0.915, p-value = 0.0028) between an increased intensity in pimonidazole

and low sO_2 measured using photoacoustic imaging, although with a different tomographic PAI system to that used in this study. In 2016, Tzoumas et al. [44], using the MSOT (from iThera) system, also showed good congruence between pimonidazole staining distribution and low blood sO_2 measurements. The pimonidazole staining from our study, Fig. A 4, showed the presence of extensive tumour hypoxia, as has been observed previously using histology and BOLD-MRI with the same tumour model [45]. The pimonidazole distribution was generally in good spatial agreement with blue regions (Fig. A 4), i.e., low sO_2, in the PAI 'oxymaps'. Fig. A 4 also showed that black pixels in the PAI, where the level of haemoglobin falls below the noise threshold of the MSOT, or very dark blue regions (sO_2~0) probably correspond with necrotic regions, as seen in H&E images (A&D). This was expected since regions of depleted of vasculature rapidly become necrotic and acellular. Nevertheless, due to the different slice thicknesses of the techniques (10 μm for histology and 900 μm for PAI), it is not possible to perfectly co-register the two types of images and this may lead to discrepancies. This direct comparison between histology and PAI is also not possible because both modalities are used at different time points. PAI is done *in vivo*, while histology processing is done *ex vivo* and the samples are frozen and excised 45 minutes after imaging, which can contribute to differences between modalities, since hypoxia is variant in time. Despite of the challenges to achieve exact co-registration between histology and MSOT images, the pimonidazole stained tumour sections clearly demonstrated the potential of PAI to infer the spatial heterogeneity in hypoxia in tumours.

The photoacoustic signal variability over 75 minutes was measured to investigate whether the injectable anaesthesia could affect haemoglobin and blood sO_2 measured in tumours. Fig. A 5 show a decreasing trend of the black pixels, regions where HbT is too low to be measured, after the first 10 minutes of imaging. Shah et al. [23] showed, by co-registration of PAI (using this system) and microbubble contrast-enhanced ultrasound images, that the black regions in tumours (in mice) corresponded to regions with low levels of perfusion, defined as regions where the injected microbubbles took longer to arrive compared to the other better perfused regions within the tumour.

Parallel to a decreasing trend in the percentage of black pixels, an increase in in Hb, HbO_2 and HbT (Fig. A 5 and Table A 1) was also measured over the 75 minute imaging, resulting in increased blood sO_2 for 3 out of 4 animals. These results suggest peripheral vasodilation. The combination of medetomidine, fentanyl and midazolam used for this study has been shown to cause a significant increase in blood pressure in rabbits and rats, which could arise from an increase in vascular resistance or peripheral vasoconstriction, [46, 47]. However, it is well-known that the cardiovascular effects of the combination of these anaesthetic agents vary in different species [48] and to the authors' knowledge, there have been no reports on its effect in female $FOXnu^{n1}$ mice. The increase in HbT and sO_2 in our study can be due to a

cardiovascular effect of the anaesthetic agent combination; due to an influence of the hydrodynamic pressure, when the animal is enveloped in a plastic film and submerged inside the water tank; or due to an influence of the compression of the tumour due to the animal's body weight, which possibly stops blood outflow from the tumour. All these factors could have contributed to the trend that was observed and further work is necessary to understand its source.

Table A 2 shows the quantification of the variation in the blood sO_2 and haemoglobin components over the 75 minutes imaging study. The inter- and intra- tumour CoVs were similar in this study, >16.0±8.4% and >20.9±3.1%, respectively, regarding the parameters analysed: Hb, HbO_2, HbT and sO_2. This reflects a high variation in the measured signal of each animal, expected due to the increasing trend in haemoglobin and blood sO_2 over time. Joseph et al. (2017) [32] studied the repeatability and reproducibility of PAI with the same system used for this paper in the left kidney and spleen of 8-12 week old mice (n=7), acquiring images over a period of 90 minutes, under isoflurane anaesthesia. The authors found a steady increasing trend in HbT and blood sO_2 over the 90 minute imaging acquisition. The group reported that the intra-organ CoVs for haemoglobin (Hb, HbO_2 and HbT, measurements averaged over a single ROI) for spleen was below 16.4 and for kidney below 18.5, while for sO_2 these values dropped to 3.9 and 3.4, respectively. The CoVs measured in this paper during 75 minutes of imaging in subcutaneous tumours were higher than those measured in spleen and kidney, although it is not possible to compare the uncertainties in the measurements. In Joseph et al. experiment, the organs (spleen and left kidney) are located internally in the animal's body, so there is probably minimal compression of their blood supply due to mounting in the system, unlike what happens for subcutaneous tumour, located in the periphery. This is in addition to the deficient vascular supply that renders tumours prone to 'cyclic' hypoxia [2], which can affect the measurements of haemoglobin and oxygen saturation.

In the second study, the effects of re-positioning the animal three times during one imaging session were also analysed. Fig. A 6 shows that the size and shape of the tumour may vary considerably during repositioning of the animal, changing the size of the tumour-ROI used for analysis. Subcutaneous tumours, besides being subject to compression due to the animal's body weight acting against buoyancy, as well as due to hydrostatic pressure, can move relative to underlying anatomy as the skin can be highly mobile. Therefore, during longitudinal studies it would be important for the user to try and place the tumour in the same position relative to the MSOT mouse holder. From Fig. A 6, it is possible to observe differences in the 'oxymaps' depending on the position of the animal, which can result in differences in the distribution and intensity of blue/red pixels. In one animal, mouse 4, in position 2, imaging resulted in an atypical high number of black pixels (46%**Error! Reference**

source not found.), correlating with uncharacteristically low levels of Hb, HbT and sO_2. Ideally, the tumour should be in the direct direction of the laser beam. However, with this system, this implies that the tumour is being compressed, besides the thin film and surrounding water, by the animal's weight, which can further constrict the blood supply to the tumour. This is a potential explanation to what was observed for animal 4. Therefore, placing the animal at a slight angle can be an option. Further, after placing the animal in the tank, if a high number of black pixels is observed, the animal should be removed and re-positioned to improve signal detection. In case this is not detected during imaging, scans should be excluded when percentage of black pixels is above 30%.

In order to investigate if the differences in 'oxymaps' during the re-positioning study also resulted in significant differences in ROI-averaged photoacoustic imaging measurements (Hb, HbO_2, HbT and sO_2) over time, the changes in these measurements were also calculated. Fig. A 7and Table A 4: Summary of average slice- and intra-tumour CoV of the measurements after repositioning each animal 3 times, during air-breathing imaging, and the average Hb, HbO_2, HbT and sO_2. show a trend for an increase in Hb, HbO_2, HbT and sO_2 over time, during the re-positioning study. The signal change reported in Table 4 shows a similar change for animals 1 to 3 for the haemoglobin components (range of 0.0094 to 0.019 for haemoglobin components and of 0.00041 to 0.0051 for sO_2) compared to that calculated for the 75 minute study (range of 0.0071 to 0.030 for haemoglobin components and of 0.00025 to 0.0031 for sO_2). A trend for a decrease or constant percentage of black pixels over time, in each position, was also observed for animals 1 to 3, as observed in the 75 minute imaging study. Animal 3 exhibited no trend in levels of sO_2 compared to the other two animals, consistent with the observations of the sequential imaging for a period of 75 minutes. Table A 4 shows that for this study, the p-values were >0.05 so the slopes (change in signal) were not significantly different from zero. This is likely due to the scarce (n=3 positions) number of points, per animal.

From Figs. B2-B5, it is also possible to observe there were no statistical differences between the slopes representing the change in photoacoustic imaging measurements between the re-positioning and the 75 minute imaging study. This suggests that repositioning the animal does not significantly increase the variability in the variation of the ROI-averaged measurements, but instead time under anaesthesia seems to have a larger impact on the PAI studies. The imaging for animal 4, in position 2 that resulted in a large amount of black pixels, increased the inter- and intra-tumour CoV for the re-positioning study. However, the majority of the signal in this imaging scan was lost, so it is not possible to know if this decrease is a result of changes in the tumour or simply an artefact due to the signal loss.

The inter- and intra-tumour CoV for the CAL^R tumours due the re-positioning of the animal, in Table A 4, were >22.0±21.2% and >26.5±8.3%, respectively, for all the parameters (Hb,

HbO_2, HbT and sO_2), hence similar to those obtained for the study without re-positioning the animal (see Table A 2), over a 75 minute period, apart from animal 4. This also suggests that anaesthesia is the main experimental factor that contributes for the variability of the signal.

The 6 day longitudinal study of CAL^R tumours showed no temporal trend in sO_2 or haemoglobin (Hb, HbO_2 and HbT) (Fig. A 8), i.e. no increase or decrease in these parameters was consistently measured over time for all animals. Tomaszewski et al. [41] used oxygen enhanced (OE)-PAI, to visualise the spatiotemporal heterogeneity of tumour vascular function in a poorly differentiated and aggressive prostate tumour model, PC3. They showed that sO_2 (while O_2 breathing) and ΔsO_2 (difference in measured sO_2 between air- and oxygen-breathing) decreased with tumour growth, from a 30 mm^3 volume to time of culling. The CAL^R model used for this project has also been shown to be aggressive [36] and hypoxic, using MRI and histology evidence (pimonidazole for hypoxia and Hoechst staining for perfusion) [49], so a decrease in sO_2, as observed by Tomaszewski et al. [41], might have been expected. However, this was not the case, either during air- or oxygen-breathing imaging, for the CAL^R tumour model.

The intra- and inter-tumour CoVs for the 6 day imaging study, Table A 5, were >19.3±8.7% and >27.0±4.1%, respectively, for the haemoglobin parameters (Hb, HbO_2 and HbT). The sO_2 parameter showed less intra-tumour CoV (7.5±2.5%) in the long term studies, in comparison to Hb, HbO_2 and HbT. Joseph et al. [32] also demonstrated, by imaging the animals on 3 consecutive days, that while the sO_2 was constant over time in kidney (maintained between 0.8 and 0.7) and spleen (maintained between 0.6 and 0.8), for HbT the variation was larger (between 25-16 A.U and 9-13 A.U. for spleen and left kidney, respectively). These studies suggest that variation in blood sO_2 is expected to be lower compared to that for haemoglobin. Also, the intra-tumour blood sO_2 variability is less for the long-term study, over 6 days, compared to that obtained for the 75 minute (16.0±8.4%) and re-positioning (22.0±21.2%) studies, once more showing that time under anaesthesia, per imaging session, should be minimised.

In order to assess whether there was any dependence of tumour blood sO_2 on tumour growth, the growth rates of the 10 CAL^R tumours during two different growth stages, were calculated using the exponential-linear model. The goodness of fit showed a good correlation (R^2>0.8) between the model and 8 datasets. Of the two animals omitted from analysis, one of the tumours became ulcerated, which is known to introduce an error in tumour measurement [50] and the other animal showed an unexpected delay in tumour growth. Fig. A 9**Error! Reference source not found.** shows a good linear relationship between the linear growth rate and the variation in sO_2 (R^2 = 0.72, n=8), during oxygen-breathing. A good linear relationship was also found between the rate of change in volume calculated just for the 6 days of imaging and percentage change in sO_2 (R^2 = 0.67). Tumours that grew faster (n=5)

during the linear phase ($\alpha 1 > 20$ mm.day^{-1}) had a decrease in sO_2 [range of -10% to -56%] between days 1 and 6 of imaging, probably because they outgrew their blood supply before new vasculature could be formed. Slower growing tumours (n=3) exhibited an increase or no change in sO_2 [+12% and -1%], possibly because angiogenesis was occurring at a rate similar to the tumour growth rate. In this study, oxygen proved to be a good contrast agent to show the differences between tumours.

This novel study evaluated the baseline variation in the photoacoustic signal over the short (up to 75 mins) and long (6 day) term in a subcutaneous head and neck tumour model. The intrinsic variability in these growing tumours may be useful in the future when studying changes in oxygenation following different therapies in this tumour model, such as radiotherapy and HIFU. Other tumour types might show different variation. For example, Tomaszewski et al. [41] showed differences in the haemodynamic behaviour assessed by PAI in two different prostate tumour models, PC3 and LNCaP.

Some recommendations follow up from this paper:

1. Given the time dependence of the imaging parameters, due to anaesthesia, to perform inter- and intra-animal comparison in longitudinal studies, ideally the imaging should be started at a fixed time point after anaesthesia.
2. Whenever applicable, to image sham treated animals at the same time points as treated ones, particularly in longitudinal studies to investigate the resultant effects of therapies in amount of haemoglobin or blood sO_2.
3. If a high percentage of black pixels is seen during the scan, the animal should be removed and re-positioned to obtain more PAI signal. Also, exclusion of datasets where the majority of signal in the tumour has been lost, when this was not perceived by the user during the imaging session.
4. Another alternative is to image a nearby healthy organ and use this data for normalising each tumour dataset.

5. Conclusions

This paper describes the variation in haemoglobin (Hb, HbO_2 and HbT) and oxygen saturation over short (up to 75 minutes) and long (6 days) periods of time, in subcutaneous head and neck tumours in nude mice. Time under anaesthesia is the largest source of variability in the photoacoustic signal. With a carefully planned experimental setup, photoacoustic imaging could be used for assessing changes in tumour haemoglobin and oxygenation in longitudinal studies, including those designed to assess cancer therapies that may affect vasculature and, consequently, tumour oxygenation.

Supplemental figures and tables

Fig. B1: ROI-averaged percentage of black pixel, and Hb, HbO_2, HbT and sO_2 signals, for CAL^R tumours (n=4) imaged after being removed and re-positioned in the tank three times, during oxygen-breathing. Error bars represent the standard deviation over 3 adjacent central tumour slices, 1 mm apart. Solid lines represent a linear regression fitted to the data.

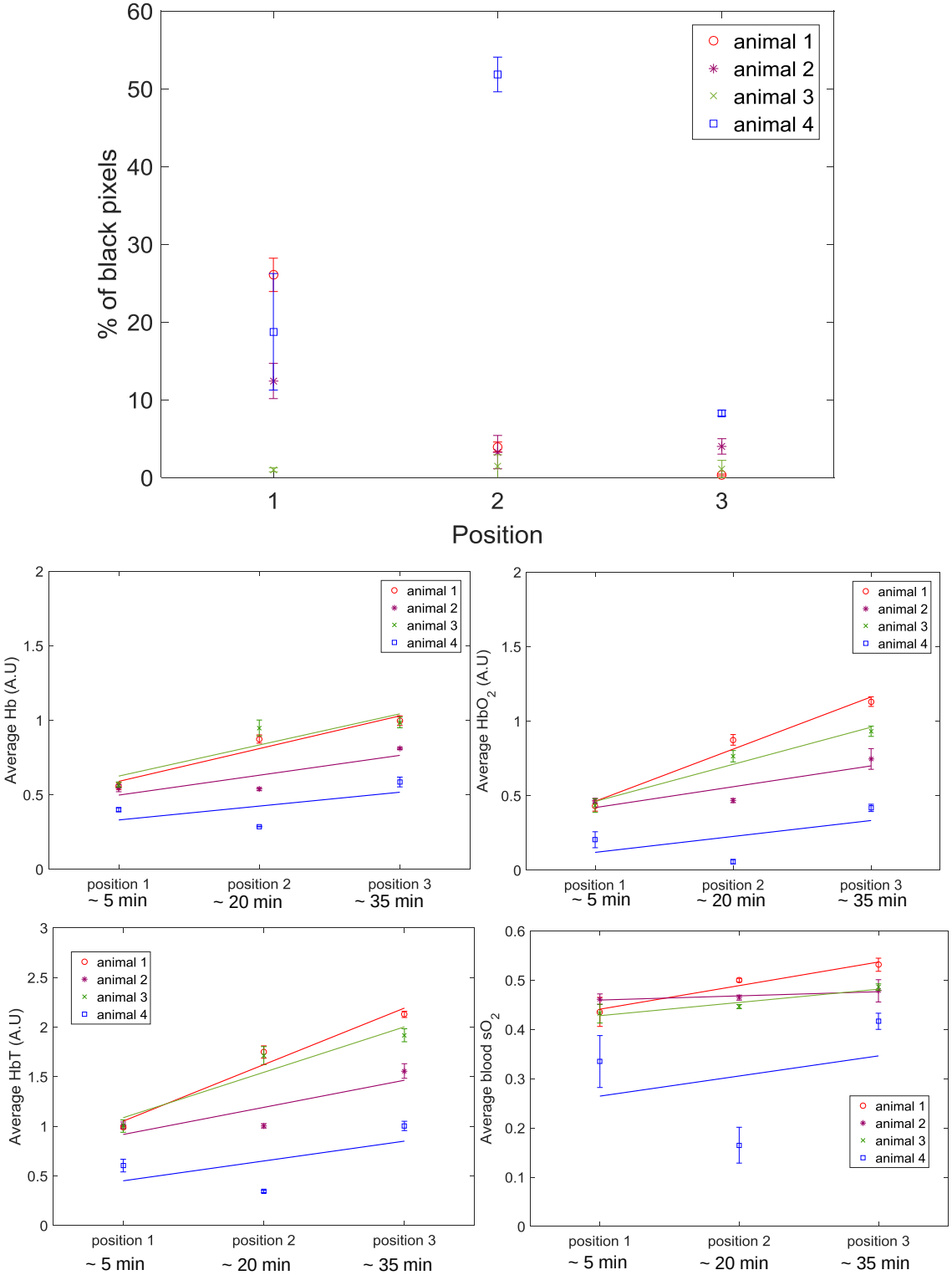

Table B1: Average Hb, HbO_2, HbT and sO_2 signal change, during the short term re-positioning study (oxygen-breathing).

Animal		Signal change, min^{-1} (95% CI)	R^2	p-value	SSE
1	Hb	0.015 (-0.033, 0.062)	0.939	0.158	0.006
	HbO_2	0.023 (-0.022, 0.069)	0.977	0.098	0.006
	HbT	0.038 (-0.055, 0.13)	0.964	0.121	0.024
	sO_2	0.0032 (-0.0049, 0.011)	0.962	0.126	<0.001
2	Hb	0.0089 (-0.060, 0.077)	0.732	0.348	0.013
	HbO_2	0.0093 (-0.059, 0.078)	0.752	0.333	0.013
	HbT	0.018 (-0.12, 0.15)	0.742	0.339	0.051
	sO_2	0.00057 (-0.0021, 0.0032)	0.883	0.228	<0.001
3	Hb	0.014 (-0.070, 0.098)	0.817	0.281	0.020
	HbO_2	0.017 (-0.023, 0.057)	0.965	0.120	0.004
	HbT	0.031 (-0.093, 0.15)	0.908	0.197	0.043
	sO_2	0.0018 (-0.0044, 0.0079)	0.932	0.160	<0.001
4	Hb	0.0062 (-0.094, 0.11)	0.380	0.579	0.028
	HbO_2	0.0071 (-0.12, 0.13)	0.346	0.601	0.043
	HbT	0.0084 (-0.20, 0.22)	0.208	0.589	0.141
	sO_2	0.0027 (-0.10, 0.11)	0.101	0.793	0.030

Table B2: Summary of average slice- and intra-tumour CoV of the measurements after repositioning each animal 3 times, during oxygen-breathing imaging, and the average Hb, HbO_2, HbT and sO_2.

Animal	Parameter	average (±std)	Intra-tumour CoV (%)	Average Slice-CoV (%)
1	Hb	0.81±0.23	28.0	3.5±0.5
	HbO_2	0.81±0.35	43.6	5.0±2.7
	HbT	1.62±0.58	35.8	2.1±1.3
	sO_2	0.49±0.05	10.0	3.4±3.1
2	Hb	0.63±0.16	24.7	2.4±1.8
	HbO_2	0.56±0.16	28.8	5.2±3.6
	HbT	1.19±0.32	26.6	3.4±1.3
	sO_2	0.47±0.01	1.9	2.7±1.8
3	Hb	0.83±0.23	27.7	4.2±1.3
	HbO_2	0.71±0.25	35.7	6.4±3.7
	HbT	1.54±0.48	31.1	5.0±1.4
	sO_2	0.45±0.03	6.1	2.2±1.9
4	Hb	0.42±0.15	35.6	3.2±2.4
	HbO_2	0.23±0.18	80.12	19.4±11.7
	HbT	0.65±0.33	51.1	6.3±3.7
	sO_2	0.31±0.13	42	13.9±9.2
4 (excluding position 2)	Hb	0.49±0.12	26.7	4.4±2.6
	HbO_2	0.31±0.15	48.5	16.0±14.4
	HbT	0.80±0.28	35.2	7.6±4.2
	sO_2	0.38±0.06	15.4	9.8±8.3
Average intra-tumour CoV (n=4)	Hb	29.0±4.6		
	HbO_2	47.1±22.9		
	HbT	36.1±10.6		
	sO_2	15.0±18.3		
Average intra-tumour CoV (without position 2 for mouse 4) (n=4)	Hb	26.8±1.5		
	HbO_2	39.2±8.7		
	HbT	32.2±4.2		
	sO_2	8.4±5.7		

Fig. B2: Comparison of Hb change between longitudinal (75 minute) and re-positioning studies. p-values indicate if the differences between the two slopes resultant from a linear model fitting are statistically significant (if p-value<0.05).

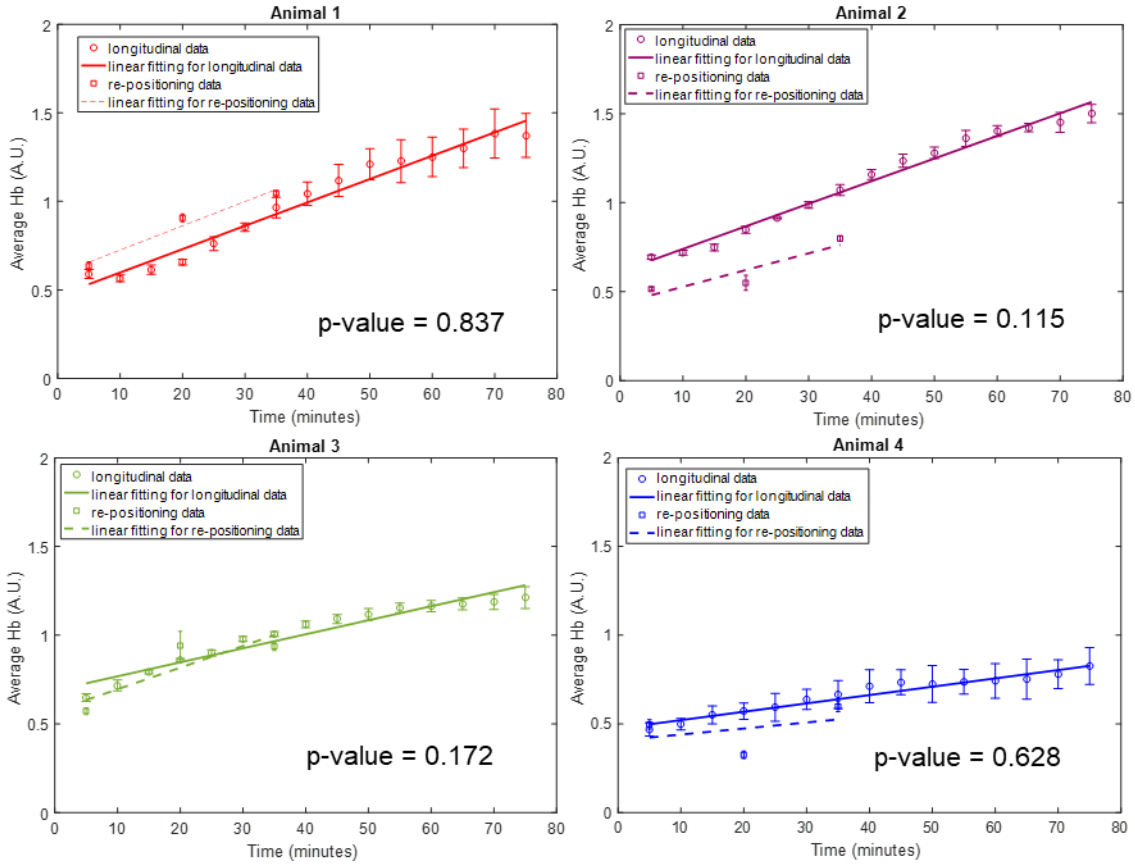

Fig. B3: Comparison of HbO_2 change between longitudinal (75 minute) and re-positioning studies. p-values indicate if the differences between the two slopes resultant from a linear model fitting are statistically significant (if p-value<0.05).

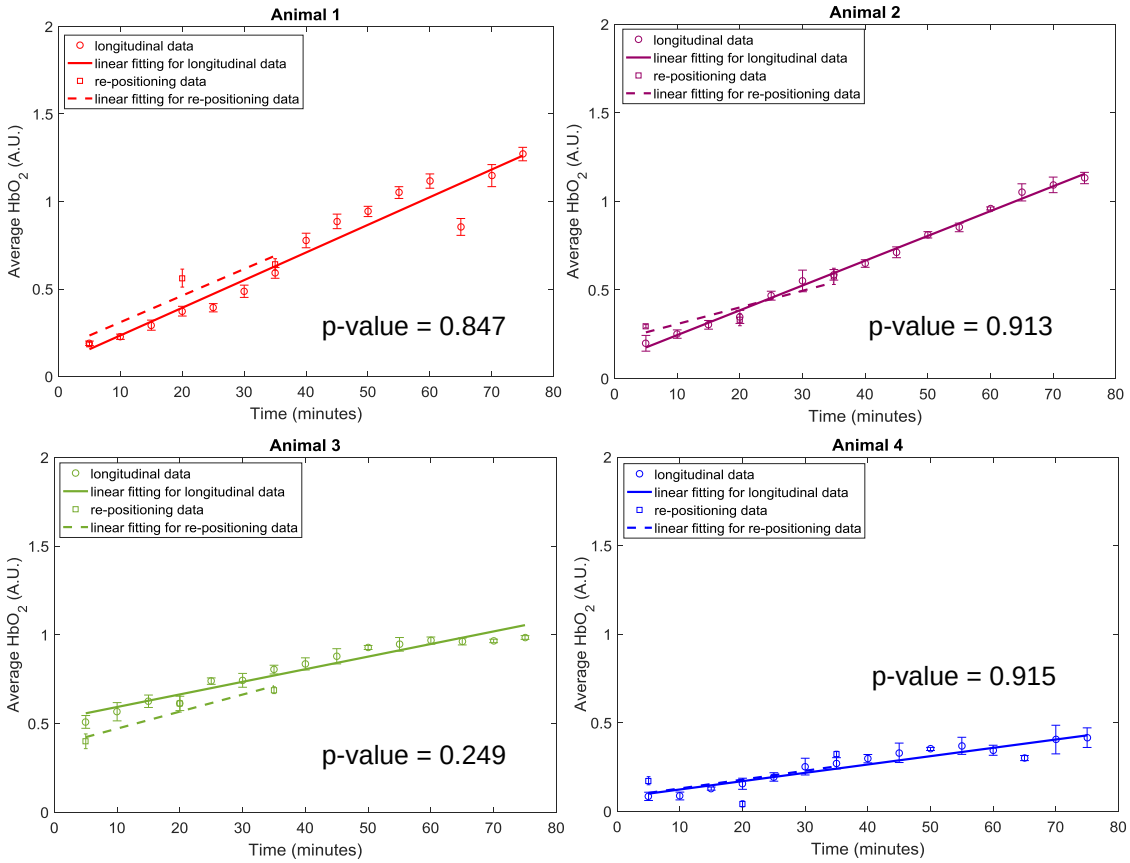

Fig. B4: Comparison of HbT change between longitudinal (75 minute) and re-positioning studies. p-values indicate if the differences between the two slopes resultant from a linear model fitting are statistically significant (if p-value<0.05).

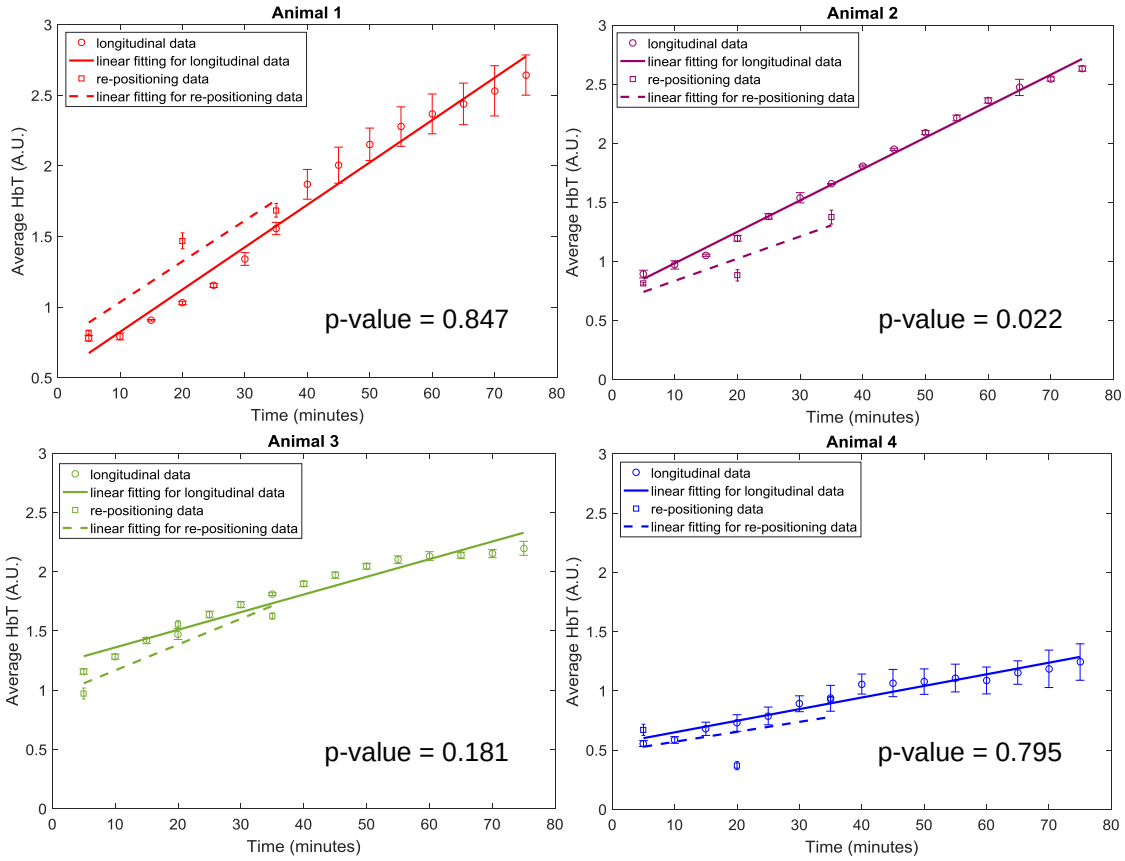

Fig. B5: Comparison of sO_2 change between longitudinal (75 minute) and re-positioning studies. p-values indicate if the differences between the two slopes resultant from a linear model fitting are statistically significant (if p-value<0.05).

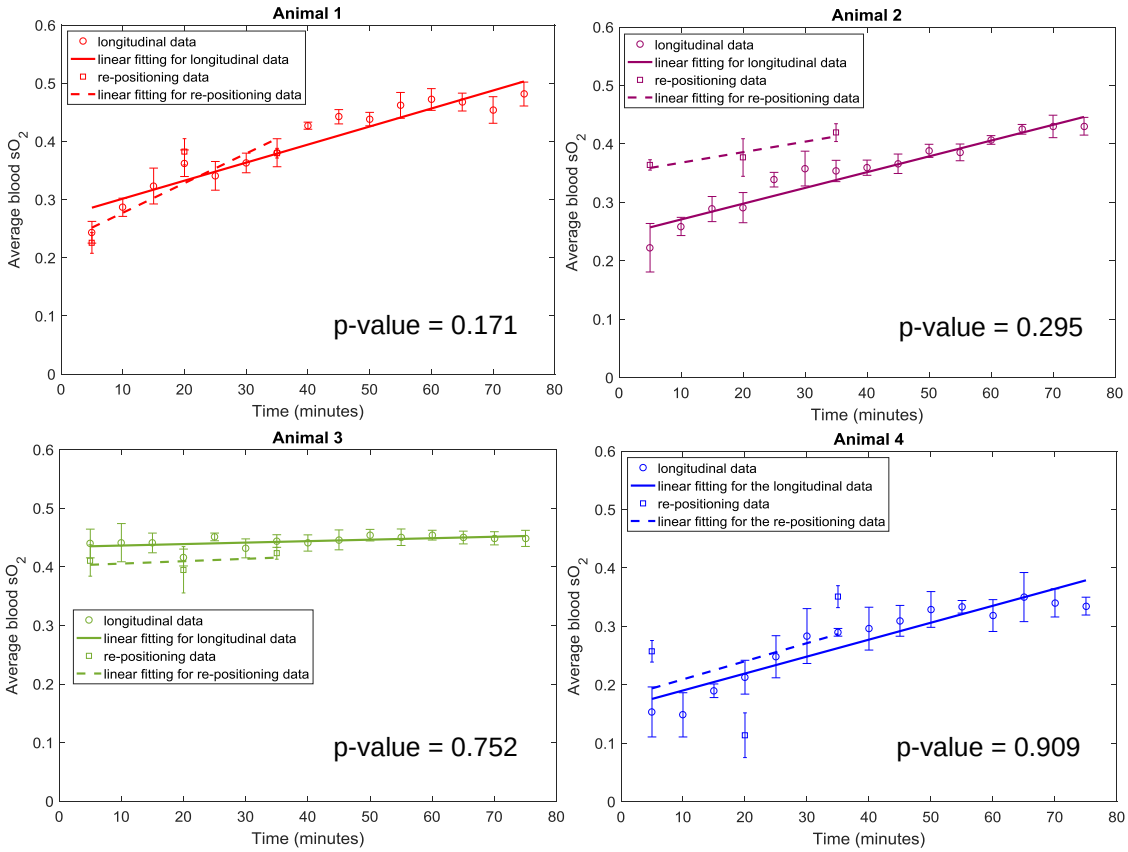

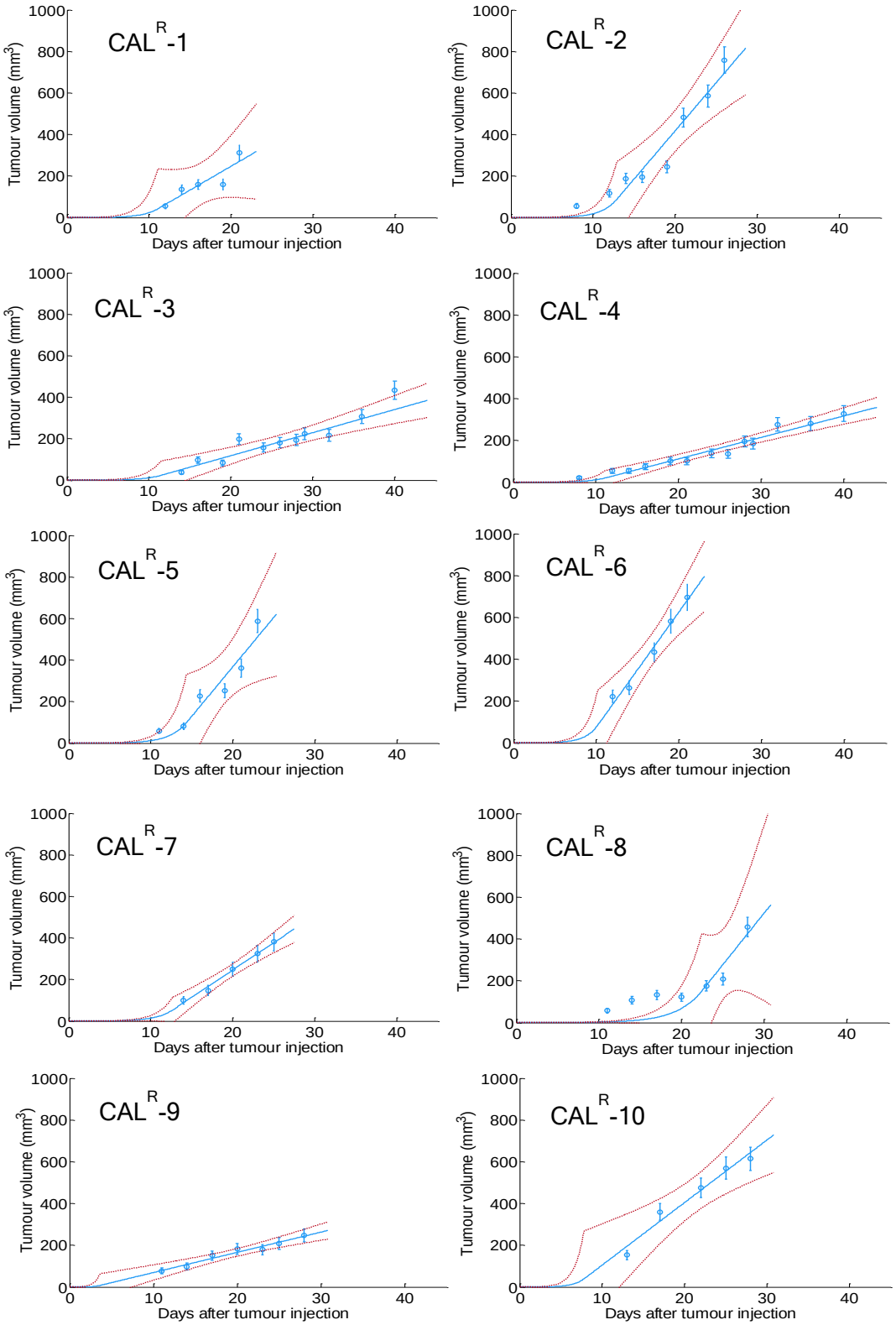

Fig. B6: CAL^R tumour volume, as measured by calipers (blue circles). Error bars represent tumour volume error, as described by Eq. A 2. The exponential-linear fitted model is shown by the blue full line with 95% confidence intervals (dashed red lines).

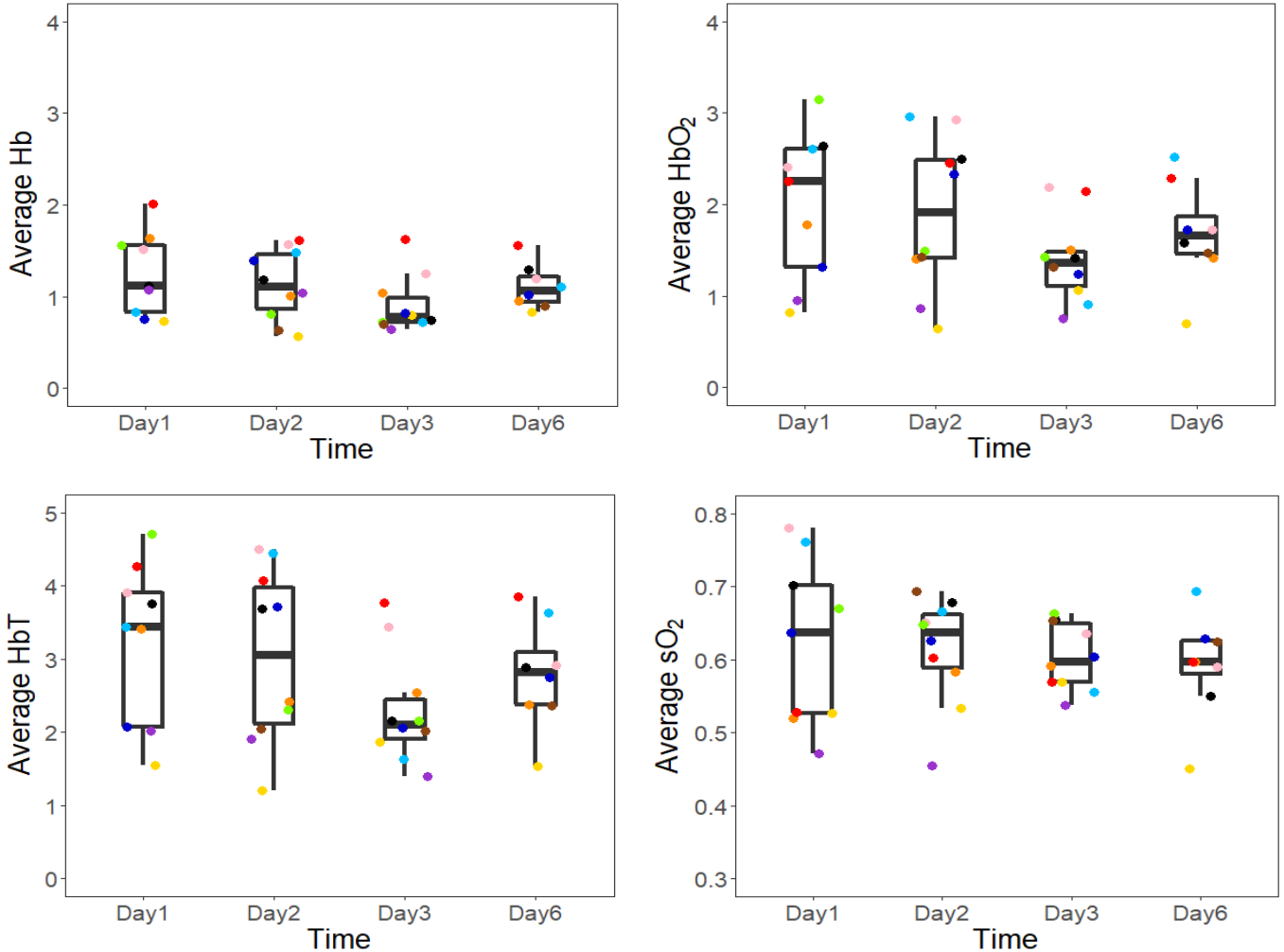

Fig. B7: Average haemoglobin and blood sO_2 values for the 3 central tumour slices of 10 CAL^R tumours, over a 6 day imaging period, for air-breathing imaging. Day 1 corresponds to the time at which tumours reached approximately 200 mm^3. The whisker plots shows the distribution of the measurements; the central black line in each box represents the median of the population; top and bottom horizontal lines in each box represent the upper and lower quartile and the whiskers the minimum and maximum values.

Table B3: Summary of inter- and intra-tumour CoVs for the CAL^R tumours (N=10), over a 6 day period, for ROI-averaged Hb, HbO_2, HbT and sO_2, during oxygen-breathing imaging.

Parameter	Intra-tumour CoV (%)	Inter-tumour CoV (%)
Hb	41.2±15.2	29.8±5.6
HbO_2	19.5±11.7	35.9±4.5
HbT	22.4±11.7	31.3±4.4
sO_2	6.5±3.2	11.8±3.6

Acknowledgements

We gratefully thank the Portuguese Foundation for Science and Technology (PhD grant SFRH/BD/90250/2012) for funding part of this project. We further acknowledge funding from the EPSRC (strategic equipment grant EP/NO15266/1) and the Cancer Research UK Cancer Imaging Centre at the Institute of Cancer Research (grant C1060/A16464). We would also like to thank the Focused Ultrasound Foundation for their support of our Centre of Excellence.

References

1. Krock, B.L., N. Skuli, and M.C. Simon, *Hypoxia-induced angiogenesis: good and evil.* Genes Cancer, 2011. **2**(12): p. 1117-33.
2. Michiels, C., C. Tellier, and O. Feron, *Cycling hypoxia: A key feature of the tumor microenvironment.* Biochim Biophys Acta, 2016. **1866**(1): p. 76-86.
3. Dewhirst, M.W., *Relationships between cycling hypoxia, HIF-1, angiogenesis and oxidative stress.* Radiat Res, 2009. **172**(6): p. 653-65.
4. Collins, J.A., et al., *Relating oxygen partial pressure, saturation and content: the haemoglobin-oxygen dissociation curve.* Breathe (Sheff), 2015. **11**(3): p. 194-201.
5. Rockwell, S., et al., *Hypoxia and radiation therapy: past history, ongoing research, and future promise.* Curr Mol Med, 2009. **9**(4): p. 442-58.
6. Harada, H., *[Hypoxia-inducible factors as molecular targets for cancer therapy].* Nihon Rinsho, 2012. **70 Suppl 8**: p. 113-7.
7. Yoshimura, M., et al., *Microenvironment and radiation therapy.* Biomed Res Int, 2013. **2013**: p. 685308.
8. Peeters, S.G., et al., *A comparative study of the hypoxia PET tracers [(1)(8)F]HX4, [(1)(8)F]FAZA, and [(1)(8)F]FMISO in a preclinical tumor model.* Int J Radiat Oncol Biol Phys, 2015. **91**(2): p. 351-9.
9. Peeters, S.G., et al., *Current preclinical and clinical applications of hypoxia PET imaging using 2-nitroimidazoles.* Q J Nucl Med Mol Imaging, 2015. **59**(1): p. 39-57.
10. Lopci, E., et al., *Imaging acute spinal myelitis with 18F-FDG PET/CT.* Eur J Nucl Med Mol Imaging, 2014. **41**(2): p. 399-400.
11. Tatum, J.L., et al., *Hypoxia: importance in tumor biology, noninvasive measurement by imaging, and value of its measurement in the management of cancer therapy.* Int J Radiat Biol, 2006. **82**(10): p. 699-757.
12. Zhao, D., et al., *Comparison of 1H blood oxygen level-dependent (BOLD) and 19F MRI to investigate tumor oxygenation.* Magn Reson Med, 2009. **62**(2): p. 357-64.
13. Chopra, S., et al., *Comparing oxygen-sensitive MRI (BOLD R2*) with oxygen electrode measurements: a pilot study in men with prostate cancer.* Int J Radiat Biol, 2009. **85**(9): p. 805-13.
14. Baudelet, C. and B. Gallez, *How does blood oxygen level-dependent (BOLD) contrast correlate with oxygen partial pressure (pO2) inside tumors?* Magn Reson Med., 2002. **48**(6): p. 980-6.
15. Hoskin, P.J., et al., *Hypoxia in prostate cancer: correlation of BOLD-MRI with pimonidazole immunohistochemistry-initial observations.* Int J Radiat Oncol Biol Phys, 2007. **68**(4): p. 1065-71.
16. Prasad, P., et al., *Evaluation of renal hypoxia in diabetic mice by BOLD MRI.* Invest Radiol, 2010. **45**(12): p. 819-22.
17. Beard, P., *Biomedical photoacoustic imaging.* Interface Focus, 2011. **1**(4): p. 602-31.
18. Gerling, M., et al., *Real-time assessment of tissue hypoxia in vivo with combined photoacoustics and high-frequency ultrasound.* Theranostics, 2014. **4**(6): p. 604-13.
19. Xu, M.H. and L.H.V. Wang, *Photoacoustic imaging in biomedicine.* Review of Scientific Instruments, 2006. **77**(4).

20. Raes, F., et al., *High Resolution Ultrasound and Photoacoustic Imaging of Orthotopic Lung Cancer in Mice: New Perspectives for Onco-Pharmacology.* PLoS One, 2016. **11**(4): p. e0153532.
21. Ueda, S., et al., *Baseline tumor oxygen saturation correlates with a pathologic complete response in breast cancer patients undergoing neoadjuvant chemotherapy.* Cancer Res, 2012. **72**(17): p. 4318-28.
22. Mallidi, S., et al., *Prediction of tumor recurrence and therapy monitoring using ultrasound-guided photoacoustic imaging.* Theranostics, 2015. **5**(3): p. 289-301.
23. Shah, A., et al., *Value of combining dynamic contrast enhanced ultrasound and optoacoustic tomography for hypoxia imaging.* Photoacoustics, 2017. **8**: p. 15-27.
24. Rich, L.J. and M. Seshadri, *Photoacoustic imaging of vascular hemodynamics: validation with blood oxygenation level-dependent MR imaging.* Radiology, 2015. **275**(1): p. 110-8.
25. Rich, L.J. and M. Seshadri, *Photoacoustic monitoring of tumor and normal tissue response to radiation.* Sci Rep, 2016. **6**: p. 21237.
26. Li, M.L., et al., *Simultaneous molecular and hypoxia imaging of brain tumors in vivo using spectroscopic photoacoustic tomography.* Proceedings of the Ieee, 2008. **96**(3): p. 481-489.
27. Shah, J., et al., *Photoacoustic imaging and temperature measurement for photothermal cancer therapy.* J Biomed Opt, 2008. **13**(3): p. 034024.
28. Gray, J.P., et al., *Multi-Wavelength Photoacoustic Visualization of High Intensity Focused Ultrasound Lesions.* Ultrason Imaging, 2016. **38**(1): p. 96-112.
29. Yao, D.K., et al., *Photoacoustic measurement of the Gruneisen parameter of tissue.* J Biomed Opt, 2014. **19**(1): p. 17007.
30. Tzoumas, S., et al., *Eigenspectra optoacoustic tomography achieves quantitative blood oxygenation imaging deep in tissues.* nature communications, 2016.
31. Maslov, K., H.F. Zhang, and L.V. Wang, *Effects of wavelength-dependent fluence attenuation on the noninvasive photoacoustic imaging of hemoglobin oxygen saturation in subcutaneous vasculature in vivo.* Inverse Problems, 2007. **23**(6): p. S113-S122.
32. Joseph, J., et al., *Evaluation of Precision in Optoacoustic Tomography for Preclinical Imaging in Living Subjects.* J Nucl Med, 2017. **58**(5): p. 807-814.
33. Shaw, C.J., et al., *Pathophysiological mechanisms of high-intensity focused ultrasound-mediated vascular occlusion and relevance to non-invasive fetal surgery.* J R Soc Interface, 2014. **11**(95): p. 20140029.
34. Park, H.J., et al., *Radiation-induced vascular damage in tumors: implications of vascular damage in ablative hypofractionated radiotherapy (SBRT and SRS).* Radiat Res, 2012. **177**(3): p. 311-27.
35. Hellevik, T. and I. Martinez-Zubiaurre, *Radiotherapy and the tumor stroma: the importance of dose and fractionation.* Front Oncol, 2014. **4**: p. 1.
36. Box, C., et al., *A novel serum protein signature associated with resistance to epidermal growth factor receptor tyrosine kinase inhibitors in head and neck squamous cell carcinoma.* Eur J Cancer, 2013. **49**(11): p. 2512-21.
37. Benzekry, S., et al., *Classical mathematical models for description and prediction of experimental tumor growth.* PLoS Comput Biol, 2014. **10**(8): p. e1003800.

38. Simeoni, M., et al., *Predictive pharmacokinetic-pharmacodynamic modeling of tumor growth kinetics in xenograft models after administration of anticancer agents.* Cancer Res, 2004. **64**(3): p. 1094-101.
39. Rosenthal, A., D. Razansky, and V. Ntziachristos, *Fast semi-analytical model-based acoustic inversion for quantitative optoacoustic tomography.* IEEE Trans Med Imaging, 2010. **29**(6): p. 1275-85.
40. Kneipp, M., et al., *Functional real-time optoacoustic imaging of middle cerebral artery occlusion in mice.* PLoS One, 2014. **9**(4): p. e96118.
41. Tomaszewski, M.R., et al., *Oxygen Enhanced Optoacoustic Tomography (OE-OT) Reveals Vascular Dynamics in Murine Models of Prostate Cancer.* Theranostics, 2017. **7**(11): p. 2900-2913.
42. Ellingsen, C., et al., *DCE-MRI of the hypoxic fraction, radioresponsiveness, and metastatic propensity of cervical carcinoma xenografts.* Radiotherapy and Oncology, 2014. **110**(2): p. 335-341.
43. Rademakers, S.E., et al., *Metabolic markers in relation to hypoxia; staining patterns and colocalization of pimonidazole, HIF-1alpha, CAIX, LDH-5, GLUT-1, MCT1 and MCT4.* BMC Cancer, 2011. **11**: p. 167.
44. Tzoumas, S., et al., *Eigenspectra optoacoustic tomography achieves quantitative blood oxygenation imaging deep in tissues.* Nat Commun, 2016. **7**: p. 12121.
45. L. C. J. Baker, et al. *Evaluating imaging biomarkers of acquired resistance to targeted EGFR therapy in xenograft models of human squamous cell carcinoma of the head and neck (SCCHN)*. in *American Association for Cancer Research*. 2013. Washington, DC., USA.
46. Baumgartner, C., et al., *Effects of medetomidine-midazolam-fentanyl IV bolus injections and its reversal by specific antagonists on cardiovascular function in rabbits.* Can J Vet Res, 2010. **74**(4): p. 286-98.
47. Albrecht, M., et al., *Influence of repeated anaesthesia on physiological parameters in male Wistar rats: a telemetric study about isoflurane, ketamine-xylazine and a combination of medetomidine, midazolam and fentanyl.* BMC Vet Res., 2014. **10**(310).
48. Albrecht, M., et al., *Effects of isoflurane, ketamine-xylazine and a combination of medetomidine, midazolam and fentanyl on physiological variables continuously measured by telemetry in Wistar rats.* BMC Vet Res, 2014. **10**: p. 198.
49. Panek, R., et al., *Noninvasive Imaging of Cycling Hypoxia in Head and Neck Cancer Using Intrinsic Susceptibility MRI.* Clinical Cancer Research, 2017. **23**(15): p. 4233-4241.
50. Workman, P., et al., *Guidelines for the welfare and use of animals in cancer research.* Br J Cancer, 2010. **112**(11): p. 1555-1577.